Applied Energy 382 (2025) 125285

Contents lists available at ScienceDirect

Applied Energy

journal homepage: www.elsevier.com/locate/apenergy

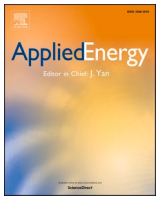

Energy performance and crop yield production of a semitransparent photovoltaic greenhouse

A. Moreno [a], D. Chemisana [a,*], E.F. Fernández [b]

[a] Applied Physics Section of the Chemistry, Physics and Environmental Science Department, University of Lleida, Lleida 25001, Spain
[b] Advances in Photovoltaic Technology (AdPVTech), CEACTEMA, University of Jaén, Las Lagunillas Campus, Jaén 23071, Spain

HIGHLIGHTS

- Integration of two semitransparent OPV modules in a multi-tunnel greenhouse.
- A holistic model is carried out to assess energy, light, and crop behaviour.
- Two typical greenhouse-based locations are analysed: Almeria and Agadir.
- 66 % coverage is the optimal configuration balancing energy savings and crop growth.

ARTICLE INFO

Keywords:
Flexible photovoltaics
Agrivoltaics
Organic photovoltaics (OPVs)
Greenhouse
Semitransparent photovoltaics

ABSTRACT

Agrivoltaics have emerged as a viable solution to resolve conflicts arising from land-use competition between large photovoltaic solar installations and conventional agriculture. However, their implementation has not yet fully addressed the issue of social community rejection due to visual impact or making agricultural tasks more difficult. For this reason, integrating photovoltaics into existing agricultural infrastructure could offer a promising solution to mitigate this issue. The present research focuses on the analysis and modelling about the integration of two types of semitransparent organic photovoltaic (OPV) modules in multi-tunnel greenhouses. Two different representative locations of high density of greenhouses are selected: Almeria (Spain) and Agadir (Morocco). A holistic model based on Python/Trnsys/Radiance/TOMGRO is proposed to evaluate the energy, light, and tomato crop behaviour under various OPV coverage percentages and their positions on the greenhouse roof. The results demonstrate that higher OPV coverage percentages lead to a reduction in overall energy consumption in both locations. However, when looking at the illumination levels and weight of the tomato crop the tendency is opposite, resulting in insufficient illumination levels for some periods. This scenario presents a significant challenge in determining the optimal solution, owing to the difficulty in striking a balance between two essential goods: energy and food. In response to this, a strategy that slightly favours food production is adopted, aiming to minimise the impact on crop growth. From this perspective, the optimal solution for both locations is the use of OPV modules with 66 % coverage. This configuration is projected to satisfy about 50 % of the heating energy needs, but it may lead to a reduction in tomato yields by around 12 % with respect to a standard greenhouse.

1. Introduction

Climate change, the unsustainable consumption of natural resources, and the degradation of ecosystems are interconnected challenges that are deeply influenced by both the current energy model and agricultural practices. The energy sector is undergoing a transition to a renewable energy-based model, and among all renewable resources, solar energy is the most abundant. Solar photovoltaics (PVs) are the fastest-growing energy conversion method. However, the relatively low generated power density of solar PV requires installations to occupy large areas of land, creating significant land-use competition, particularly in areas where agricultural activities are prevalent [1]. In the case of agriculture, the transition to a sustainable model is expected to be more difficult. Taking into account that projections indicate a population growth of up to 9.1 billion in 2050 [2], a substantial increase in the demand for basic

* Corresponding author.
E-mail address: daniel.chemisana@udl.cat (D. Chemisana).

https://doi.org/10.1016/j.apenergy.2025.125285
Received 20 April 2024; Received in revised form 4 December 2024; Accepted 3 January 2025
Available online 13 January 2025

Nomenclature

$a(\lambda)$	plant action spectrum, dimensionless
A	Area, m^2
A_{wind}	Window area, m^2
C_d	Discharge coefficient, dimensionless
c	Speed of light, m/s
C_w	Wind effect coefficient, dimensionless
$D_F(T_d)$	Function of fruit development rate, dimensionless
DU	Distribution uniformity, dimensionless
$E(\lambda)$	AM 1.5 solar spectral irradiance, $W/m^2/nm$
E_v	Coefficient of effectiveness of the openings, dimensionless
$f_F(T_d)$	Function to modify partitioning to fruit for average daily temperature, dimensionless
G_{CROP}	Crop Growth Factor, dimensionless
G	Global incident irradiance, W/m^2
g_e	Transpiration conductance, m/s
GR_{net}	Above ground biomass growth rate, $g/m^2/day$
$g(T_d)$	Function to reduce growth due to high daytime temperature, dimensionless
h	Planck's constant, J·s
I	Irradiance, W/m^2
I_B	Beam irradiance, W/m^2
I_{diff}	Diffuse irradiance, W/m^2
K_m	Maximum spectral efficiency, lm/W
k_F	Development time from first fruit to first ripe fruit, days
L	Amount of energy needed to evaporate water for a leaf, J/g
LAI_{max}	Maximum possible leaf area index, m^2 leaf/m^2 ground
m_{vent}	Air flow rate through the openings, m^3/h
N_A	Avogadro's constant, mol^{-1}
N	Node, dimensionless
N_b	Coefficient in expolinear equation, dimensionless
N_{FF}	Begins node position, dimensionless
N_m	Maximum rate of node appearance, nodes/day
P	Power output, W
$P_{RQE}(\lambda)$	Relative Quantum Efficiency
Q_{trans}	Heat gain of transpiration, W/m^2
T_{cell}	Cell temperature, °C
$T_{cell,STC}$	Cell temperature under Standard Test Conditions, °C
TF	Thermal Factor, dimensionless
U_o	Wind speed, m/s
V_{max}	Maximum increase in vegetative tissue dry weight growth per node, g/node
$V(\lambda)$	Human eye photopic response, dimensionless
W	Total plant dry weight, g
W_f	Total fruit dry weight, g
W_m	Total mature fruit dry weight, g
W_{rel}	Relative spectral power distribution, dimensionless
χ_{air}	Absolute water vapour concentration of greenhouse air, g/m^3
χ_{crop}	Absolute water vapour concentration at crop level, g/m^3
α_F	Maximum partitioning of new growth to fruit, dimensionless
η_{OPV}	OPV efficiency, dimensionless
$\lambda(T_d)$	Temperature function to reduce the rate of leaf area expansion, dimensionless

Greek letters

α	Absorptance at wavelength λ, dimensionless
β	Coefficient in the expolinear equation of LAI, dimensionless
γ	Power temperature coefficient, %/°C
δ	Maximum leaf area expansion per node, m^2/leaf/node
$\Delta\lambda$	Wavelength interval, nm
θ	Transition coefficient between vegetative and full fruit growth, dimensionless
ρ	Reflectance at wavelength λ, dimensionless
ρ_{plant}	Plant density, plants/m^2
τ	Transmittance at wavelength λ, dimensionless
χ	Absolute water vapour concentration, g/m^3
φ	Radiant flux, W

Abbreviations and acronyms

AOIF	Angle of Incidence Factor
AVT	Average Visible Transmittance
APT	Average Photosynthetic Transmittance
COP	Coefficient of Performance
DLI	Daily Light Integral
DSSC	Dye Sensitised Solar Cell
ETFE	Ethylene Tetrafluoroethylene
GHI	Global Horizontal Irradiance
HLQ	Highest Lower Quartile
LAI	Leaf Area Index
NIR	Near Infrared
OPV	Organic Photovoltaic
PAR	Photosynthetically Active Radiation
PCE	Power Conversion Efficiency
PPFD	Photosynthetic Photon Flux Density
PV	Photovoltaic
R2R	Roll to Roll
RQE	Relative Quantum Efficiency
SPD	Spectral Power Distribution
STC	Standard Test Conditions
SMARTS	Simple Model of the Atmospheric Radiative Transfer of Sunshine
TMY	Typical Meteorological Year
UV	Ultraviolet

goods, including food products, is expected to rise by 70 % in 2050 [3]. Furthermore, the conventional agricultural practices will deal with various conflicts: having enough land (conflicts with other uses) and fresh water, and the ecological impacts of the current intensive agricultural model. These conflicts are contributing to destabilising the Earth system and situating the agriculture as a significant or major contributor to change the planetary boundaries beyond their "safe and just limit" into risk zones [4–6]. In this context, a process of transformation towards innovative and "holistic" approaches, such as agroecology, agrivoltaics and climate-smart agriculture is taking place. These approaches aim at increasing the productivity on existing agricultural land while protecting biodiversity and ecosystem processes. This principle is referred to as "Sustainable Intensification" [6].

The concept of agrivoltaics, which involves co-locating agriculture and photovoltaic installations, has emerged as a promising solution [7,8]. It enables the maximization of crop yields, minimization of water usage, and production of resilient renewable energy [9]. The scientific community has increased its efforts to study and experimentally investigate possible solutions, focusing primarily on short-term forecasts and identifying a no recognised standard of assessment [10]. There are different classifications of agrivoltaic systems, normally based on the position of the solar panels and crops: crops between photovoltaic rows, crops under photovoltaic panels and the use of photovoltaics in greenhouses [11–13]. The integration of photovoltaic systems within greenhouses is an increasingly recognised solution to mitigate the high energy consumption required to maintain a stable and controlled indoor

microclimate. Furthermore, certain photovoltaic technologies can replace conventional greenhouses covering materials or shading devices. This integration can effectively avoid the problems associated with visual impact, which may occasionally lead to opposition against agrivoltaic installations. [14].

Various photovoltaic technologies can be employed for integration into greenhouses, contingent upon the specific greenhouse type and the interior lighting requirements. In Southern European countries, plastic film-covered greenhouses are widely utilised and can be classified based on various shapes such as tunnel greenhouses, pitched roof greenhouses, arc-shaped roof greenhouses, and Parral-type greenhouses [15]. The mechanical characteristics of solar cells become particularly significant when they are intended to be part of the covering material. It should be noted that the use of flexible panels is generally limited to the 2nd generation (thin film) and 3rd generation (emerging PV) solar cells [16]. Regardless of the cladding material utilised, incorporating semitransparency is crucial in greenhouse covering. The achievement of semitransparency in solar modules can be performed through two primary approaches: the pattern-based technique, using opaque cells, and the penetration-based technique using semitransparent cells. It is also noteworthy that semitransparency can be achieved in photovoltaic systems through optical concentrators.

Initially, the technology incorporated in greenhouses was based on crystalline silicon photovoltaics. Several studies specifically focused on investigating the influence of solar panel orientation and the patterns used to achieve semitransparency [17–23]. The primary issues associated with this technology revolve around shading, which consequently leads to a decrease and non-uniform distribution of photons with wavelengths between 400 and 700 nm, which is referred to as photosynthetically active radiation (PAR). The studies based on thin-film modules are still limited and primarily focused on amorphous silicon [24,25]. Even though they can achieve semitransparency in the active layer, amorphous silicon overlaps with the absorption of the PAR spectrum. To overcome this weakness, research focusing on emerging systems that allow spectral selection is gaining importance [26]. Notable among these are wavelength-selective focusing lenses [27–29], which, despite their innovative approach to spectral management, face challenges such as high initial costs and ongoing maintenance expenses. Luminescent solar concentrators [30–32] represent another promising avenue; however, they have historically grappled with low power conversion efficiency. Dye-sensitised solar cells (DSSCs) [33,34], still in the experimental stage and not yet ready for commercialization, offer unique advantages in terms of spectral selection due to their colour variation characteristics. OPVs offer numerous potential advantages, making them particularly intriguing for various applications. These advantages include flexibility, processability, low material cost, and independence from scarce resources. A particularly interesting feature of OPVs is the ability to tune their absorption characteristics by adjusting the composition of the active layer materials. This adaptability allows for customization according to specific light transmission requirements. Recent advancements in OPV cells technology have shown promising results. Power conversion efficiency has reached more than 19 % in small area opaque cells [35] and semitransparent cells have reached 10 % efficiency with 50 % visible transparency [36].

In the literature, two distinct lines of research concerning the use of OPVs in greenhouses can be identified. The first one focuses on materials science, with the objective of simultaneously improving the electrical efficiency and transparency of OPV cells. The second research line focuses on performance evaluation, which involves assessing the effectiveness of OPV modules within actual greenhouse conditions. Such evaluations are typically conducted using a combination of experimental studies and computational modelling. Considering the objective of this study, a more detailed review of modelling greenhouse environments with the integration of semitransparent OPVs is presented.

Within the first line of research, noteworthy studies include the comprehensive review by Zhao et al. [37] on semitransparent OPV cells for agricultural applications. Their work provides a summary of power conversion efficiency (PCE) and average visible transmittance (AVT) associated with current methods and strategies of OPV cells design. In this way Meitzner et al. [38] presented a comprehensive review of the most commonly used active layer materials in OPV cells and analysed their overlap with the absorption spectrum of chloroplasts. Based on their findings, they concluded that the absorption range of the active layer of OPV cells are suitably aligned with that of plants. Wang et al. [39] focused on developing high-performance, spectrally engineered semitransparent OPV cells specifically designed for greenhouse applications. The team achieved impressive PCEs of 17.71 % in opaque devices and 13.02 % in semitransparent devices. Additionally, they demonstrated a high plant growth factor of 26.3 % with the semitransparent devices.

The studies related to the experimental evaluation of OPVs in greenhouses are conducted over specific periods to assess the electrical, thermal, lighting and crop behaviour under functional semitransparent OPVs or mock OPV-filters in real greenhouse or controlled chamber boxes [40–47]. In general, these studies indicate that installing OPVs in greenhouses not only extends their operational lifetime but also, during the hottest months, provides shading that creates more suitable climatic conditions for the growth of crops like tomatoes and lettuce.

In terms of modelling greenhouse environments with the integration of semitransparent OPVs. Okada et al. [48] presented a simulation model to assess the lettuce crop yield (based on Both et al. [49]) electric energy production in a greenhouse equipped with OPV films (PCE = 3.3 % and AVT = 30 %). Their results showed that a 49 % roof coverage with OPVs could fulfil the energy requirements of the evaluated greenhouse. Ravishankar et al. [50] studied the benefits of integrating two types of OPVs, differing only in their active layer (PCE ≈ 10 % and AVT ≈ 36 %). They developed a comprehensive energy balance model in Matlab to model the net energy demand of greenhouses. The results revealed that these integrated systems can achieve an annual surplus of energy, particularly in warm and moderate climates. Waller et al. [51] presented a practical methodology based on Rinocheros/Grasshopper and PVlib-python library to estimate the incident solar irradiance on curved surfaces. They assessed the performance of semitransparent roll-to-roll (R2R) printed OPV arrays installed on a high tunnel greenhouse with a gothic-arch roof profile. Dipta et al. [52] analysed the potential of semitransparent OPVs (PCE = 9.4 % and AVT = 24.6 %) through light simulation using Honeybey/Radiance and studied tomato crop growth based on the TOMGRO model. Their findings indicated a significant 46 % increase in the dry ground weight of tomato crops grown under semitransparent OPVs compared to those grown under conventional silicon solar cells. Ravishankar et al. [53] conducted an analysis of 64 different OPV active layers with varying roof coverage in 25 distinct climates using a dynamic energy model implemented in Matlab. In addition to solar power generation, the model integrates a comprehensive assessment of greenhouse environmental factors, such as temperature, humidity, and lighting, along with a functional plant growth model of tomato (TOMGRO) and lettuce based on Goudriaan [54]. Their study demonstrated that OPV-integrated greenhouses can achieve net-zero energy consumption in 11 different climates when cultivating lettuce and in 10 climates when cultivating tomatoes. Moreno et al. [55] presented a study involving electric, thermal, and lighting models based on the Python/Trnsys/Radiance environment to analyse the effects of covering the greenhouse roof with semitransparent OPVs (PCE = 2.8 % and AVT = 10.18 %) in Barcelona and Paris. Their findings revealed that when 50 % and 25 % of the greenhouse roof is covered by OPVs in Barcelona and Paris, respectively, illumination levels reach optimum values for tomato and lettuce growth. Furthermore, the study demonstrates that integrated OPV systems can partially cover the electricity demand of the greenhouse, covering 14 % to 63 % of the demand with 25 % to 100 % OPV coverage, respectively. In contrast, for Paris, these percentages vary from 6 % with 25 % OPV coverage to 25.3 % with 100 % OPV coverage.

In light of the above, there are notably few studies that take a holistic approach, addressing both the coverage percentage and positioning of semitransparent OPVs in greenhouses, while also considering climatic conditions, light availability, energy generation, and crop behaviour. Although OPV technology is still maturing and presents certain challenges, such as relatively shorter lifespans, higher costs, and lower efficiencies (which are already the focus of extensive materials science research), the present study aims to explore the potential of employing semitransparent OPVs in agricultural greenhouses, focusing more on practical application rather than technological or material innovations. Comprehensive modelling of energy and illumination performance, as well as tomato crop growth, is conducted seeking to support informed and proper market development and to address the existing research gaps.

These performances are analysed for different configurations based on the percentage of coverage on the roof and their position of two types of OPV modules with different transmittance profiles. The simulations are conducted in two different locations, Almeria (Spain) and Agadir (Morocco), both of which are typical regions characterised by a high density of greenhouses. Regarding the structure of this article, the manuscript is divided into 5 sections. In section 1, the topic is introduced. Section 2 delves into the theory of the luminous response of plants. Section 3 examines the characteristics of the ethylene tetrafluoroethylene (ETFE) and OPV modules. Section 4 presents the modelling methodology. Once the model is introduced, the main results are discussed in Section 5 and the main conclusions of the study are stated in Section 6.

2. Light response of plants

The energy of the sun is an essential source that drives the metabolic processes and facilitates photosynthesis in plants. The solar spectrum received on the earth surface, as shown in Fig. 1a (expressed in irradiance units and quantum units), is primarily comprised of distinct wavelength regions with approximately 5 % ultraviolet (UV) radiation (250–400 nm), 45 % of PAR region (400–700 nm, this spectral region closely aligns with the visible spectrum), and ≈50 % of near infrared (NIR) radiation (700–2500 nm). The UV light directly affects plants and microorganisms, altering species-specific interactions between them [56] and stimulates the production of secondary metabolites [57]. In the NIR region of the spectrum very little energy is absorbed by vegetation and reflection increases greatly. This high reflectance in the NIR prevents plants from overheating. On the other hand, it is absorbed mainly by the greenhouse floor soil, installations, and construction elements of the greenhouse. Then, it is released again to the greenhouse air as convection heat that increases the greenhouse air temperature [58]. PAR is regarded as the most important wavelength range for plant growth and development, directly influencing the photosynthesis process and stomatal behaviour.

During photosynthesis, molecules of glucose (along with other sugars) are synthesised from the energy of light, water, and carbon dioxide, resulting in the release of oxygen as a by-product. This entire process relies on the absorption of light by various pigments, including chlorophylls and carotenoids, which are concentrated in specialised structures called chloroplasts. The process of light absorption by photosynthetic pigments is achieved through electronic excitation. When a photon of light interacts with a pigment molecule, it elevates an electron within the pigment to a higher energy state. Different pigments possess specific energy levels corresponding to different wavelengths of light. Consequently, pigments exhibit distinct absorption spectra (Fig. 1b), selectively absorbing light of particular wavelengths. For instance, Chlorophyll a (Chl a) displays absorbance peaks at 430 and 663 nm, while Chlorophyll b (Chl b) shows peaks at 453 and 642 nm. Carotenoids such as lutein, β-carotene, and zeaxanthin are additional pigments that absorb solar radiation within the 450–570 nm range. Most of the activation wavelengths are found in the blue part of the spectrum (400 to 500 nm) or in the red part (600 to 700 nm) and far-red (700 to 800 nm). Green light (500–600 nm) is absorbed to a lesser extent by these pigments; however, due to this lower absorptance, it can penetrate more deeply and excites chlorophyll deeper in the leaves [59].

The quantum yield serves as a metric for evaluating the efficiency with which pigments convert absorbed photons into chemical energy during photosynthesis. In 1972, McCree [60] conducted a comprehensive study on the wavelength efficiency of photosynthesis and established the Relative Quantum Efficiency (RQE) curve, representing the average photosynthetic response (see Fig. 1b). McCree's measurements have significantly contributed to the conceptualization of PAR. Within the spectral range from 400 to 700 nm, McCree demonstrated that light in the red region (600 to 700 nm) yielded the highest quantum efficiency for CO_2 assimilation in plants. Light in the green region (500–600 nm)

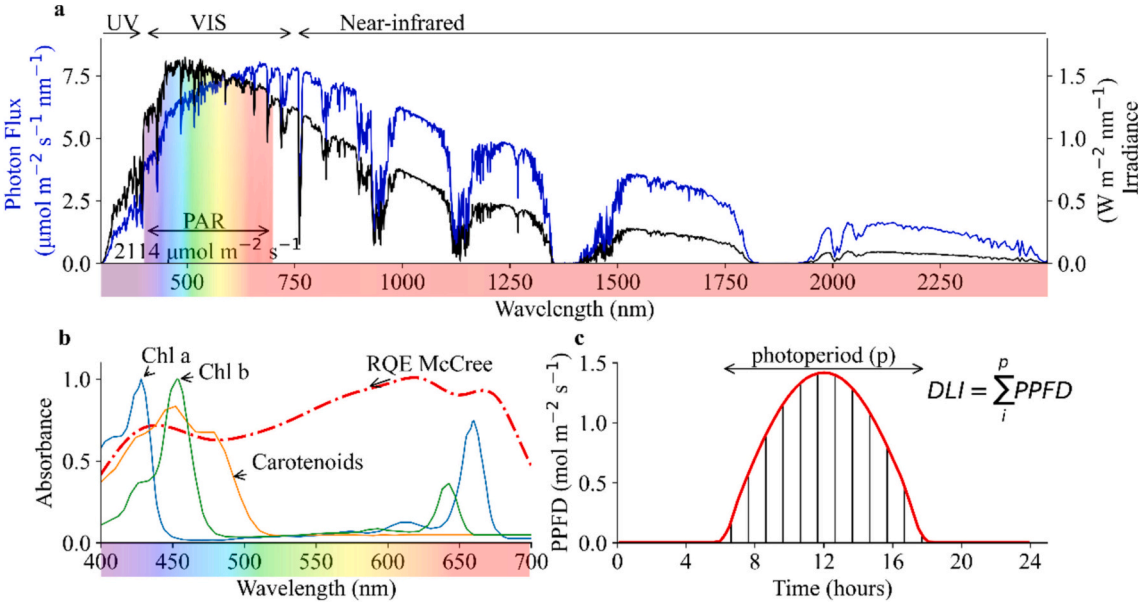

Fig. 1. a) Solar spectrum AM 1.5, a comparison of irradiance and photon flux b) Normalised absorption spectra of chlorophyll *a*, chlorophyll *b*, carotenoids and the relative quantum yield c) Daily light integral (DLI).

generally resulted in a slightly higher quantum yield compared to the blue region (400–500 nm). The lower efficiency in the blue region is attributed to internal conversion within the chlorophyll molecule, where the extra energy in blue photons, compared to red ones, is lost in the form of heat.

The quantity (irradiance levels), the light quality (light spectra) and duration of light (photoperiod) are the three parameters that influence plant growth. The commonly employed unit to measure the quantity of photons in the PAR region is the photosynthetic photon flux density (PPFD), expressed in units of μmol m^{-2} s^{-1}. The integral of the solar spectrum (AM1.5) in the PAR region corresponds to a photon flux of 2114. 30 μmol m^{-2} s^{-1}. The PPFD is an instantaneous measurement, but in the agricultural community, it is common to use the cumulative amount of light a plant receives in a day, defined as the Daily Light Integral (DLI). As depicted in Fig. 1c, this value is determined by summing the PPFD over the daylight hours of a day (photoperiod).

3. Materials

Ethylene tetrafluoroethylene (ETFE), with a thickness of 250 μm, has been considered for the transparent covering of the greenhouse. ETFE is a fluorinated polymer that has gained popularity in greenhouse and building applications due to its optical properties, durability and the relatively low amount of waste generated during its use [61].

Two R2R-printed OPV modules produced by ASCA [62] have been chosen for this study. These OPV modules are semi-transparent and flexible. In this study, these two types of OPV modules are referred to as OPV1 and OPV2. Although OPV modules are less mature and have shorter lifetimes than silicon PV, their flexibility, light weight, and tuneable transparency position them a potential candidate to be integrated in greenhouses. Moreover, based on environmental aspects OPVs are more ecofriendly than standard solar cells [63].

3.1. Optical properties of ETFE and OPV

The spectral transmittance *(τ)* and reflectance *(ρ)* of the ETFE foils and the OPV modules have been determined over a range from 0.35 to 0.9 μm with an Ocean Optics USB 4000 spectrophotometer (Ocean Optics Inc., USA) equipped with an integrating sphere. This spectral range encompasses the PAR region. Using Kirchhoff's law, the absorptance *(α)* can be derived from these experimental measurements as follows:

$$\tau(\lambda) + \rho(\lambda) + \alpha(\lambda) = 1 \tag{1}$$

The main parameter derived from the spectral measurements to indicate transmittance in literature is the Average Visible Transmittance (AVT), as defined in Eq. (2). AVT represents the weighted transmission spectrum against the photopic response of the human eyes $V(\lambda)$. However, an index that directly reflects the effect on crop growth is more reasonable. For this purpose, Emmott et al. [64] proposed the crop growth factor (G_{CROP}), as defined in Eq. (3). Here, *T(λ)* is the transmittance spectra of the OPVs and ETFE, *E(λ)* is the AM 1.5 solar spectral irradiance, and *a(λ)* represents the plant action spectrum, which is obtained from the averaged action spectrum of 27 herbaceous plants [65]. G_{CROP} factor represents the relation between the rate of photosynthesis under a semitransparent covering material to that under a clear sky. Stallknecht et al. [66] introduced an analogous metric, the Average Photosynthetic Transmittance (APT), as defined in Eq. (4), where the transmission spectrum is weighted by the RQE instead of *a(λ)*, denoted as $P_{RQE}(\lambda)$, as measured by McCree [60]. Both factors, G_{CROP} and APT, provide preliminary evaluations of how the light transmitted through semitransparent covering materials affects photosynthetic efficiency. However, it is important to note that these indicators are based on plant responses from old studies, and other interacting factors could significantly alter the effect of light quality on photosynthetic efficiency in long-term studies [67].

$$AVT = \frac{\int T(\lambda)\cdot V(\lambda)\cdot E(\lambda)\cdot d\lambda}{\int V(\lambda)\cdot E(\lambda)\cdot d\lambda} \tag{2}$$

$$G_{CROP} = \frac{\int T(\lambda)\cdot E(\lambda)\cdot a(\lambda)\cdot d\lambda}{\int E(\lambda)\cdot a(\lambda)\cdot d\lambda} \tag{3}$$

$$APT = \frac{\int T(\lambda)\cdot E(\lambda)\cdot P_{RQE}(\lambda)\cdot d\lambda}{\int E(\lambda)\cdot P_{RQE}(\lambda)\cdot d\lambda} \tag{4}$$

In addition to the previously mentioned parameters, experimental measurements can also yield colorimetric indicators, which are crucial for quantifying the colour appearance of OPVs and their impact on colour perception. Fig. 2b illustrates the CIE 1931 colour space diagram, showcasing the colour coordinates and the correlated colour temperature (CCT) of the light transmitted by both OPVs and ETFE. OPV1 exhibits a pale greyish tint with coordinates (0.321, 0.332), and its transmitted light closely matches the CIE standard illuminant D65 (0.312, 0.329), as well as the ETFE film (0.314, 0.331). The OPV2 displays a pale reddish tint, corresponding to coordinates (0.393, 0.330). The CCT values for the light transmitted by OPV1 and OPV2 are 6014 K and 3213 K, respectively. Detailed information regarding the optical characteristics of ETFE and the OPVs is provided in Table 1.

3.2. Electrical properties

Under Standard Test Conditions (STC), the efficiency values are 3.5 % for OPV1 and 3.0 % for OPV2. The power temperature coefficient *(γ)* is +0.04 % $°C^{-1}$ for OPV1 and + 0.05 % $°C^{-1}$ for OPV2. As can be seen, the power coefficients are positive, which is unusual for standard PV technologies but is a specific characteristic of OPV [68,69].

3.3. Thermal properties

The thermal properties of the greenhouse envelope have been determined based on the thermal transmittance values of ETFE, calculated in accordance with the procedure described in UNE-EN 673 [12]. The thermal conductivity, specific heat capacity and density of the ETFE components (20 °C), these values have been taken from the manufacturer: 0.24 W m^{-1} K^{-1}, 1172 J kg^{-1} K^{-} and 1700 kg m^{-3}, respectively. Based on our previous study [70], the thermal transmittance of OPV is assumed to be the same as that of ETFE.

4. Methodology

In this study, electric, thermal, lighting (illuminance) and crop growth models have been developed and analysed for the ETFE-OPV multi-tunnel greenhouse coverage The 3D model of the multi-tunnel greenhouse has been developed using the Trnsys-Sketchup plugin [71]. After creating the greenhouse model, the specifications of all materials, including those of translucent materials adapted from spectral measurements by Optics and Window programs [72] have been introduced through the Trnbuild interface. Additionally, all thermal loads in Trnbuild have been set, taking into account the evapotranspiration calculated by an external Python block. Daysim/Radiance [73] have been used to assess the lighting aspects. PVlib [74] has been used to perform simulations of the OPVs, considering irradiance, electric properties and temperature as inputs. The results obtained from the lighting simulation have been converted into quantum units through a Python script, which has been used as input in the tomato growth model (TOMGRO) [75]. Weather conditions have been obtained from Meteonorm [76]. An overview of the modelling procedure is illustrated in Fig. 3. The methodology presented in this work could similarly be adapted to other greenhouse types, PV technologies, climate conditions, and greenhouse shapes, provided that suitable 3D modelling of greenhouse structures and a detailed characterization of materials are

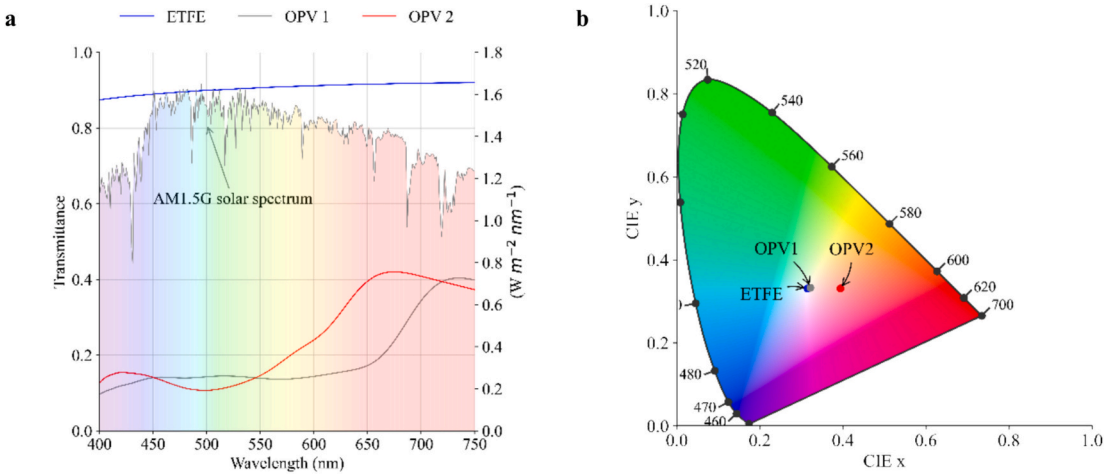

Fig. 2. a) Spectral normal transmittance of the ETFE foil (250 μm-thick) and the two OPV modules, alongside the normalised AM1.5G solar radiation spectrum. b) CIE 1931 colour space diagram showing colour coordinates of the transmitted light.

Table 1
ETFE and OPV optical characteristics.

	AVT	G	APT	CCT
OPV1	17.79	15.94	16.49	6014
OPV2	21.8	22.14	22.94	3213
ETFE	90.21	90.93	91.17	6380

conducted.

4.1. The greenhouse description

The present study involves a multi-tunnel greenhouse measuring 24 × 24 m. The greenhouse consists of three tunnels with enclosure made of stretched ETFE and a curved cover. Each tunnel chapel is 8 m wide, featuring eaves at a height of 4 m and a crest height of 6 m. The greenhouse is oriented in a north-south direction, with an average roof slope of 28.3 degrees, following the dimensions and orientation outlined in [77]. The roof curvature has been defined using three symmetric planes with slopes of 10°, 30°, and 45° to achieve the desired curvature (See Fig. 4).

The greenhouse structure is based on aluminium profiles that provide the shape, with ETFE films enclosing both the walls and the roof. In the reference case, only ETFE layers have been used for covering both the walls and the roof. The study investigates different OPVs coverage percentages, specifically 33 %, 66 %, and 100 %. These percentages have been chosen to represent a broad operational range for the OPV greenhouse system, corresponding to low, medium, and upper-limit coverage scenarios. These percentages have been applied to all possible symmetric combinations of 6-section discretised semi-circle-

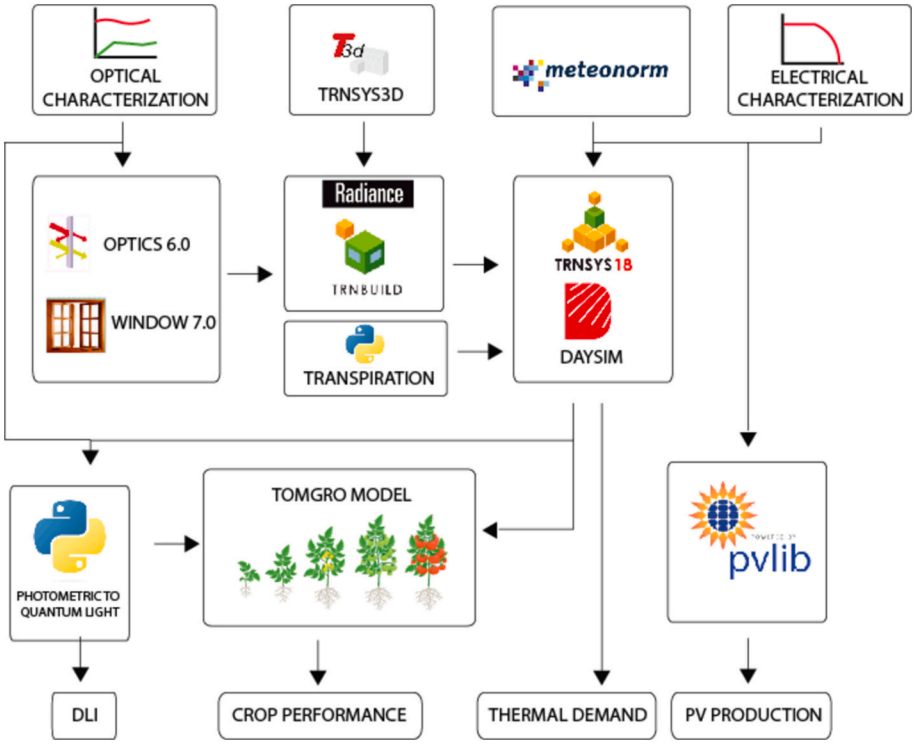

Fig. 3. Roadmap of this study and corresponding tools.

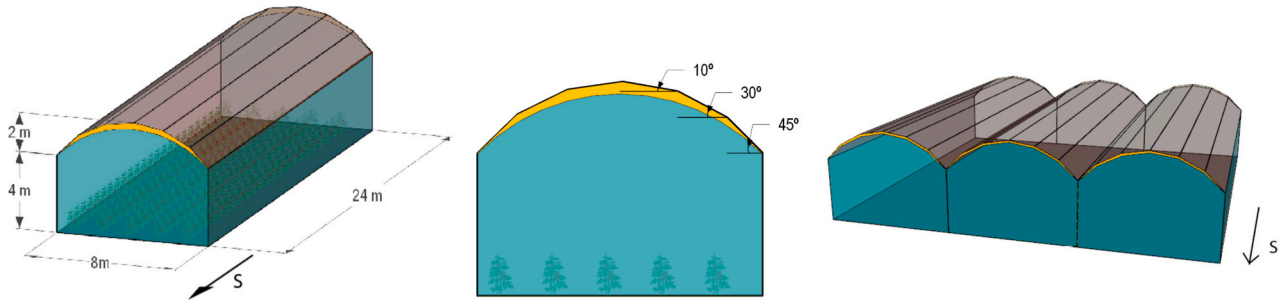

Fig. 4. The dimensions of each tunnel (left). The slopes of the symmetry planes that define the roof curvature (centre). A multi-tunnel greenhouse simulation model (right).

like roof surfaces. In total, eight configurations of the multi-tunnel greenhouse have been studied for each OPV technology (OPV1 and OPV2), including the reference case. Each configuration has been examined in the multi-tunnel setup consisting of three identical tunnels of each configuration. The studied configurations are plotted in Fig. 5 and are identified using the nomenclature introduced in Table 2.

Although the predominant greenhouse type in the analysed areas is the Parral-type greenhouse, this study focuses on multi-tunnel greenhouses, which offer greater potential for improving crop cultivation due to their better adaptation to advanced technology, allowing for more precise climate control and efficient light distribution leading to maximise the crop cycles per year [78,79]. Regarding heating systems, these are commonly implemented as a climate control strategy to prevent temperatures from dropping below critical levels (usually between 10 and 14 °C). Below this threshold plants may suffer damage and experience reduced productivity. While the vast majority of greenhouses in southern Europe remain unheated, these systems are increasingly employed in more sophisticated commercial settings [80].

4.2. Selected locations

The OPV multi-tunnel greenhouse has been evaluated in Almeria (Spain, Latitude: 36.83°, Longitude: −2.45°) and Agadir (Morocco, Latitude: 30.42°, Longitude: −9.59°). These regions manifest climatic conditions that are advantageous for greenhouse cultivation, as they are classified within the warm arid and cold arid zones, respectively, according to the Köppen-Geiger climate classification system [81]. Furthermore, in these selected locations (arid regions), preventing solar heat load from entering the greenhouse is a common and effective cooling method. This is typically achieved by using porous materials such as cloths and plastic nets, or by applying white lime to the outer surface of the greenhouse [82].

A combination of a typical meteorological year (TMY) and SMARTS [83] is utilised to generate spectral hourly radiation data. In order to incorporate the effects of cloudy days, the SMARTS spectral global horizontal irradiance values ($E_{SMARTS}(\lambda)$) are adjusted by scaling them to align with the broadband global horizontal irradiance (GHI) ones obtained from TMY data. This adjustment process follows the Eq. (5), suggested by Fernández et al. [84].

$$E(\lambda) = \frac{GHI}{\int E_{SMARTS}(\lambda)\cdot d\lambda} \cdot E_{SMARTS}(\lambda) \quad (5)$$

Table 2
ID configurations.

ID	Percentage of coverage by OPV	Angle of roof faces covered by OPV
1OPV10	33 %	10°
1OPV30	33 %	30°
1OPV45	33 %	45°
2OPV30_45	66 %	30° and 45°
2OPV10_30	66 %	10 and 30°
2OPV10_45	66 %	10 and 45°
3OPV	100 %	10°, 30° and 45°
REF	0 %	–

Fig. 6 shows the monthly cumulative global horizontal irradiance and the mean ambient temperatures. The annual cumulative GHI in Almeria is 1843.81 kWh m^{-2} and the annual average temperature is 18.93 °C while in Agadir, the annual cumulative GHI is 1849.34 kWh m^{-2} with an annual average temperature is 19.09 °C. Regarding the mean daylight illuminance on the horizontal plane (shown in Fig. 7), Almeria receives 32.22 mol m^{-2} d^{-1}, and Agadir 32.33 mol m^{-2} d^{-1}.

4.3. Greenhouse thermal model description

In order to obtain the greenhouse thermal behaviour, the 'type56b' with the TRNBuild tool of Trnsys is used. This widely used tool enables the evaluation of conventional buildings by considering various primary thermal loads in the energy balance. These loads encompass solar radiative gains, radiative losses, heat transfer through the greenhouse envelope, and heat transfer with the soil. It is important to note that the specific characteristics of the greenhouse significantly influence the magnitude of heat gains and losses. For this study, particular attention is given to the heat gains and losses attributed to ventilation and transpiration. Notably, internal sources such as human occupancy, lighting,

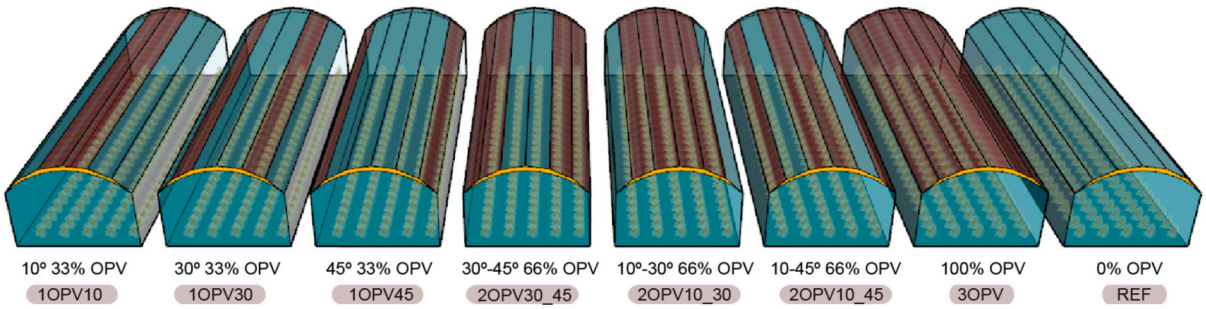

Fig. 5. The nomenclature of the multi-tunnel studied configurations based on the percentage of coverage and the position of the OPV.

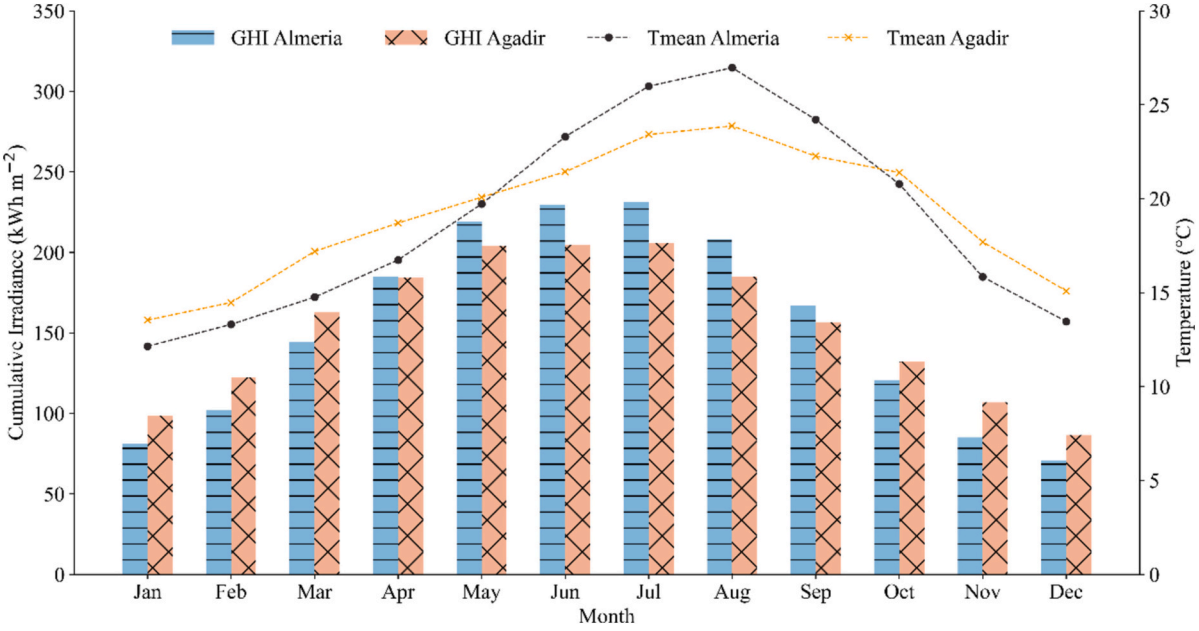

Fig. 6. Monthly irradiances and mean temperatures for Almeria and Agadir.

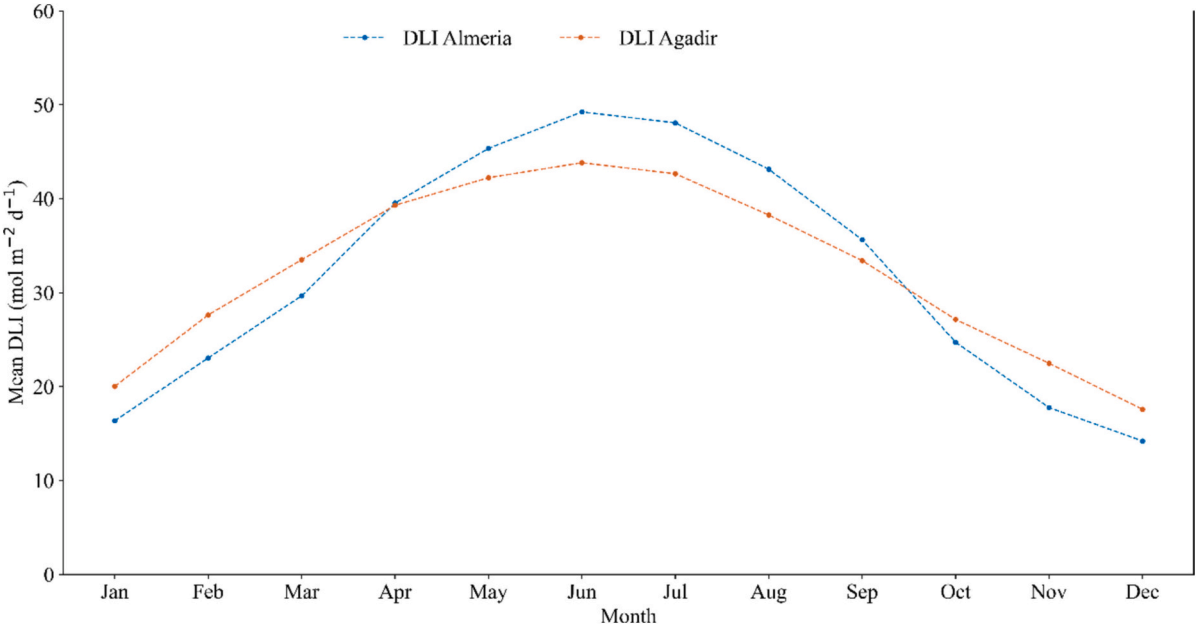

Fig. 7. Mean DLI at horizontal plane for Almeria and Agadir.

and equipment are not accounted for in the analysis.

Crop transpiration is considered by implementing the model described by Van Bevern [85] based on Penman-Monteith equation for transpiration [86]. The heat gain of transpiration is calculated as follows:

$$Q_{trans} = g_e \cdot L \cdot (\chi_{crop} - \chi_{air}) \ (Wm^{-2}) \tag{6}$$

where, χ_{crop} is the absolute water vapour concentration at crop level, while χ_{air} the absolute water vapour concentration of greenhouse air (g m^{-3}). The variable L represents the amount of energy needed to evaporate water for a leaf (J/g) and g_e represents the transpiration conductance. The comprehensive model for calculating these parameters can be found in [85].

Heat gains resulting from ventilation take into account both natural ventilation and infiltration. Natural ventilation is achieved through combined side walls and roof vents. The side walls ventilation elements are positioned around the longitudinal walls of the greenhouse, while the roof vent operates as a flap window (the variation in roof vents inclination has not been considered for the incident irradiance calculations). The total ventilation area in the greenhouse corresponds to 10 % of the total floor area. The opening and closing of these vents are controlled based on climatic conditions, specifically when the interior temperature of the greenhouse exceeds 26 °C and surpasses the ambient temperature. The flow rate through the openings is determined using an equation provided by Kittas et al. [87]:

$$m_{vent} = \frac{A_{wind}}{2} C_d \cdot \sqrt{C_w} \cdot U_o \tag{7}$$

where A_{wind} is the window area, C_d is the discharge coefficient, C_w is the wind effect coefficient and U_o is the wind speed. In the literature, it is common to use the coefficient of effectiveness of the openings, E_v, which is defined as $E_v = C_d\sqrt{C_w}$, to characterise the effect of wind on ventilation. For our research, a coefficient of effectiveness of 0.050, as obtained from [88], is utilised.

Although the incorporation of heating systems is not common in these locations, when multi-tunnel greenhouses are used, the associated technology increases their implementation [79], allowing for the combination of both long and short cultivation cycles [89]. In this study, the heating demand has been calculated based on a design temperature of 20 °C during the day and 16 °C at night throughout the heating season, which extends from October 15th to March 30th, according to the optimal values suggested by the FAO [90]. CO_2 enrichment has not been included, and the CO_2 concentration has been set at 350 ppm.

The values mentioned in the previous paragraphs are summarised in Table 3.

4.4. Model of natural light availability

The useful natural light reaching the floor of the greenhouse is modelled by the software tools Radiance 3.0 and Daysim, which are included in Trnsys 18. Daysim uses the Radiance combined with a daylight coefficient approach. It incorporates all-weather sky luminance models [91,92] and generates illuminance distributions. The primary purpose of these software tools is to calculate natural lighting or daylight in photometric units (lux). However, for photosynthesis, the light intensity received by plants is expressed in quantum light units (μmol m^{-2} s^{-1}). To convert the photometric units (illuminance) into quantum light units, two steps are required. First, the photometric units must be converted into radiometric units using Eq. (8). Subsequently, Eq. (9) should be used to convert the radiometric units into quantum light units [93].

$$\phi(\lambda) \Big/ lm = \frac{W_{rel}(\lambda)}{K_m \cdot \sum_{400}^{700} V(\lambda)\cdot W_{rel}(\lambda)\cdot \Delta\lambda} \tag{8}$$

It should be noted that λ refers to wavelengths between 400 and 700 nm, φ(λ) is the radiant flux, K_m is the maximum spectral efficiency (K_m = 683 lm/W), $W_{rel}(\lambda)$ stands for the relative spectral power distribution (SPD) of AM1.5G transmitted through semitransparent material (shown in Fig. 8), $V(\lambda)$ is the human eye photopic response and Δλ is the wavelength interval.

$$PPFD(\lambda) = \frac{\lambda\cdot\phi(\lambda)}{N_a\cdot h\cdot c} \tag{9}$$

where *N*a is Avogadro's constant, *h* stands for Planck's constant, and *c* is the speed of light.

The sum (taking into account the bandwidth of 400–700 nm) can be used as a conversion factor that relates lux (lumen m^{-2}) and PPFD (μmol m^{-2} s^{-1}):

$$PPFD = \frac{1}{N_a\cdot h\cdot c}\sum_{400}^{700}\lambda\cdot\phi(\lambda)\cdot\Delta\lambda \tag{10}$$

Table 4 includes the conversion factors calculated for the standard AM1.5 spectra and for this spectrum modified by the ETFE and OPV optical properties. It should be noted, as included in Fig. 1, that the DLI is calculated as the integral of the PPFD values over the photoperiod.

Table 3
Greenhouse model assumptions.

	Description	Value	Units
Greenhouse	Setpoint heating (day)	20	°C
	Setpoint heating (night)	16	°C
	Setpoint ventilation	26	°C
	CO2 concentration	350	ppm
	Transpiration	Q_{trans}	W m^{-2}
	Ventilation	m_{vent}	m^3 s^{-1}

To determine the spatial distribution of PPFD within the canopy, a squared grid of virtual PAR (quantum) sensors has been used to discretise the space. For this specific study, a grid interval of 0.4 m has been chosen, resulting in a total of 3360 grid elements. The positions of these virtual sensors are represented in Fig. 9. To ensure that the influence of border areas is not affecting the results, the lighting study focused solely on the central region (the central tunnel, with length between 6 m and 16 m).

The uniformity of the light distribution inside the greenhouse is a very important issue because it affects the crop production and quality. To assess the uniformity of the light inside the greenhouse the distribution uniformity (*DU*) indicator proposed by [94] is assessed. This metric is defined as the ratio of the average of the lowest quartile (H_{LQ}) to the overall average of the data (*H*), expressed as a percentage. A higher *DU* value indicates a more uniform light distribution, which is beneficial for optimising crop growth conditions.

$$DU\ (\%) = \frac{\overline{H_{LQ}}}{\overline{H}}\cdot 100 \tag{11}$$

4.5. Model of electrical production of OPV

The photovoltaic model encompasses a systematic approach aimed at determining the power output (*P*) of the OPVs configurations. This procedure follows a standard equation, denoted as Eq. (12), which takes into account various factors affecting the performance of OPV modules.

$$P = \eta_{OPV}\cdot TF\cdot\sum_{i=face} A_i\cdot G_i\cdot AOIF_i \tag{12}$$

Where *i* represents each face with the same orientation and inclination, *A* is the area, *G* is the global incident irradiance, *AOIF* is the angle-of-incidence factor that corrects the PV power when the sunrays do not fall perpendicularly on the module surface, η_{OPV} represents the OPV efficiency under Standard Test Conditions (STC), and *TF* is the thermal factor that performs the temperature correction calculated as:

$$TF = 1 + \gamma\left(T_{cell} - T_{cell,STC}\right) \tag{13}$$

where T_{cell} is the cell temperature and $T_{cell,STC}$ is the cell temperature under STC ($T_{cell,STC}$ = 25 °C). The T_{cell} is estimated from the indoor air temperature of the greenhouse.

To accurately determine the incident solar irradiance G_i and the $AOIF_i$ of the different facets of the OPV modules, the pvlib-python library has been implemented. Pvlib-python is an open-source library written in Python that offers a comprehensive set of functions and classes for simulating the performance of photovoltaic systems. The methodology employed in this process is illustrated in Fig. 10.

The solar position (zenith and azimuth) for the 15-min time step used in Trnsys has been calculated using the "get_solarposition" function from the "solarposition.py" module. The angle of incidence has been computed for each face utilising the "irradiance.aoi" function. Additionally, the various irradiance components (direct, diffuse, reflected, and global) have been determined by employing the "get_total_irradiance" function from the "irradiance.py" module. By considering the incident irradiance of each surface and applying the incident angle modifier calculated by the "iam" function, the *AOIF* (Angle of Incidence Factor) is computed as follows:

$$AOIF = \frac{I_B\cdot F(AOI) + I_{diff}}{G} \tag{14}$$

where I_B is the direct irrandiance and I_{diff} is the diffuse irradiance.

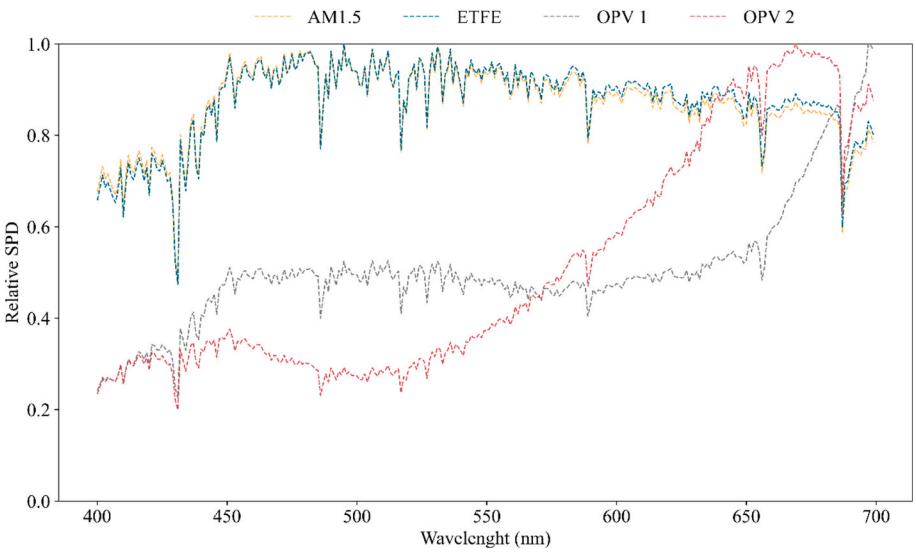

Fig. 8. Relative spectral power distribution of AM1.5G solar radiation and AM1.5G solar radiation transmitted through ETFE, OPV 1 and OPV 2.

Table 4
Conversion factor of klux to PPFD.

	Conversion factor (klux to PPFD)
AM 1.5G	18.87
AM 1.5G through ETFE	18.85
AM 1.5G through OPV1	21.31
AM 1.5G through OPV2	24.82

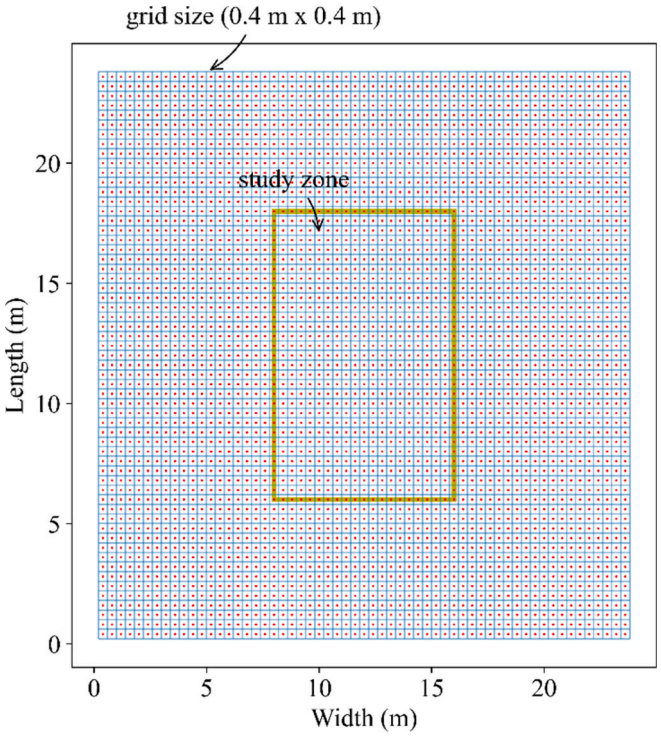

Fig. 9. Dimension of the study area and the location of measuring sensors.

4.6. Crop model

TOMGRO, developed by Jones et al. in 1991 [75], is a model used to forecast the growth and development of tomato under greenhouse based on some environmental parameters measured inside the greenhouse: air temperature, solar radiation and CO_2 concentration. This first version (1991) is complex with tremendous amounts of state variables and associated model parameters (69 state variables). In 1999, Jones et al. [95] proposed a relatively simple model for tomato growth which apparently presents a behaviour similar to the complex TOMGRO model, but with the great advantage of having only five state variables (1) node number for the main stem (N) (node); (2) Leaf Area Index (LAI) ($m^2_{leaf}\ m^{-2}_{ground}$); (3) total plant dry weight (W) ($g_{dry\ weight}\ m^{-2}_{ground}$); (4) total fruit dry weight (W_f) ($g_{dry\ weigh}\ m^{-2}_{ground}$); and (5) mature fruit dry weight (W_m) ($g_{dry\ weight}\ m^{-2}_{ground}$).

This version also included the new functions proposed by Vallejos et al. (1997) for the estimation of the effects of high temperatures on fruit growth and leaf area development. The reduced Tomgro model has been evaluated with data from several experiments and even data collected in a commercial greenhouse and the results obtained shows that the model can describe with precision the growth and production of tomato in different locations and years.

For the present work the reduced model of TOMGRO is replicated with PYTHON for solving the five state variables (dN/dt, d(LAI)/dt, dW_F/dt, dW/dt, dW_M/dt). That is defined by first order ordinary equations. $\frac{dx}{dt} = f(u,p)$, where the u vector contains the indoor conditions of the greenhouse (temperature, PPFD and CO_2) and the vector p the parameters and biological constants. In this work, plants are assumed to be well fertilised and watered. The main governing equations for calculating each state variable are presented below, for constant values and how they have been derived is available in Jones et al. (1999).

The rate of node development (dN/dt) has been modelled as:

$$\frac{dN}{dt} = N_m \cdot f_N(T) \tag{15}$$

where N_m is the maximum rate of node appearance rate and $f_N(T)$ is a function that reduces vegetative development under non-optimal temperatures.

The equation for the time changes in LAI in the reduced model can be computed as:

$$\frac{d(LAI)}{dt} = \rho_{plant} \cdot \delta \cdot \lambda(T_d) \cdot \frac{exp[\beta(N - N_b)]}{1 + exp[\beta(N - N_b)]} \cdot \frac{dN}{dt} \tag{16}$$

$$\frac{d(LAI)}{dt} = 0, when\ LAI > LAI_{max}$$

where ρ_{plant} is plant density (number of plants m^{-2} ground), δ is a

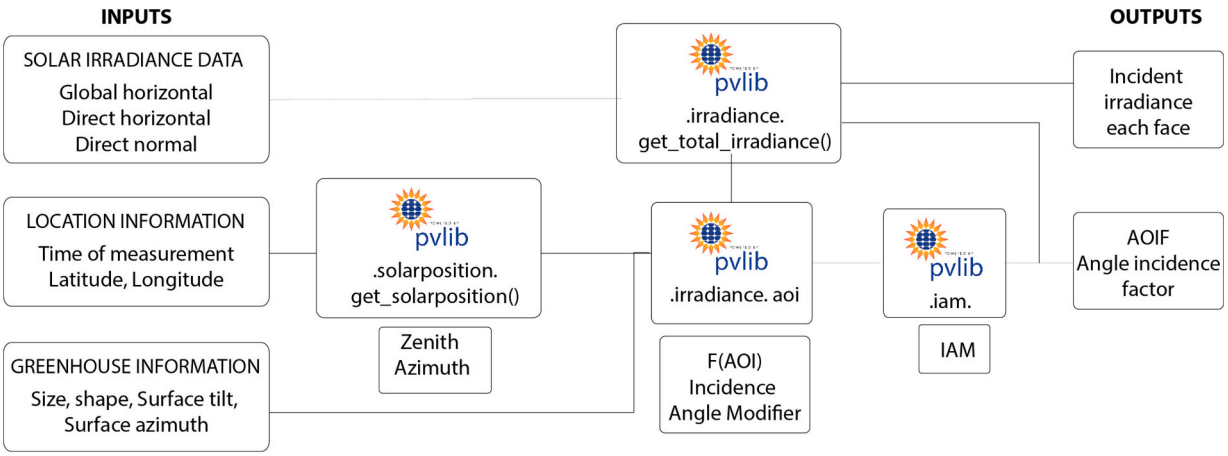

Fig. 10. Flowchart methodology to calculate the solar irradiance incident on each face of the greenhouse roof.

maximum leaf area expansion per node (m^2_{leaf} $node^{-1}$), $\lambda(T_d)$ is temperature function to reduce the rate of leaf area expansion, β and N_b are coefficients in expolinear equation and LAI_{max} is the maximum possible leaf area index (m^2_{leaf} m^{-2}_{ground}).

The above ground biomass accumulation is computed as:

$$\frac{dW}{dt} = min\left(\frac{dW_F}{dt} + (V_{max} - p_1)\cdot\rho\cdot\frac{dN}{dt}, GR_{net} - p_1\cdot\rho\cdot\frac{dN}{dt}\right) \quad (17)$$

where GR_{net} is above ground biomass growth rate, p_1 is loss leaf dry weight per node after LAI_{max} is reached and V_{max} is the maximum increase in vegetative tissue dry weight growth per node.

Partitioning of aboveground growth to fruit each day begins at node position N_{FF} and increases asymptotically to a maximum partitioning using the equation:

$$\frac{dW_F}{dt} = GR_{net}\cdot\alpha_F\cdot f_F(T_d)\cdot[1 - exp(-\theta(N - N_{FF}))]\cdot g(T_d)$$

$$if\ (N > N_{FF} + k_F) \quad (18)$$

where α_F is the maximum partitioning of new growth to fruit, $f_F(T_d)$ is a function to modify partitioning to fruit for average daily temperature, θ is the transition coefficient between vegetative and full fruit growth, $g(T_d)$ is function to reduce growth due to high daytime temperature and k_F development time from first fruit to first ripe fruit.

To move fruit from green to mature stages is calculated as:

$$\frac{dW_M}{dt} = D_F(T_d)\cdot(W_F - W_M)\ if(N > N_{FF} + k_F) \quad (19)$$

where $D_F(T_d)$ is a function of fruit development rate.

The Node development (N) and leaf area index (LAI) are solved hourly. Their values at the end of each day are used to compute the weights (W, W_f, W_m).

5. Results and discussion

In this section, the obtained results are presented in three categories: energy balance within the greenhouse, light transmission and distribution, and crop production and performance.

5.1. Thermal behaviour and electricity production

Thermal demand and electrical generation are analysed to understand how the semitransparent OPVs integrated in the greenhouse are performing and affecting the interior space conditions. Fig. 11 shows the thermal demand of the reference multi-tunnel greenhouse (without OPVs). As shown in the figure, heating is required from October to April, with lower demands in spring and autumn compared to the winter months. The annual heating demand is 45,775 kWh in Almeria and 34,177 kWh in Agadir, representing an annual energy demand per floor area surface of 79.47 kWh m^{-2} and 59.33 kWh m^{-2}, respectively. Different authors have evaluated the heating demand in greenhouses, obtaining values that depend on the control temperature, ventilation, and the treatment of the greenhouse cover. Prieto et al. [96] evaluated the thermal demand of a greenhouse for tomato production situated in Almeria with indoor air temperature for heating season was set at 12 °C, resulting in a heating demand of 25.37 kWh m^{-2}. Lopez et al. [97] analysed various strategies for night air heating on the earliness and yield of greenhouse-grown snap beans in Almeria-type greenhouse. They set the interior night temperature at 14 °C and 12 °C, resulting in a heating demands of 67.5 kWh m^{-2} and 32.4 kWh m^{-2}, respectively. Choab et al. [98], investigated the thermal behaviour and the heating/cooling energy needs of a greenhouse for tomato production in Agadir. They considered heating set-point temperatures of 21 °C during the day and 18 °C at night, obtaining a heating demand ranging from 25 kWh m^{-2} to 35 kWh m^{-2}, depending on the cover used. Considering that in the present study, the set-point temperature is defined as 16 °C during the night and 20 °C during the day, our results are in line with those of previous studies.

Different scenarios have been examined: The reference configuration uses only ETFE as covering, and other configurations involve covering with two different OPV technologies (for details, see Section 4). Fig. 12 clearly illustrates the impact of the coverage percentage, revealing that an increase in the coverage leads to higher heating demands due to lower solar gains. The positioning of the OPVs according to the different configurations studied and the OPV technology used does not significantly influence the outcome. In Almeria, an increase in the heating demand of 3.1 %, 5.8 %, and 10.6 % has been observed for coverage percentages of 33 %, 66 %, and 100 %, respectively. In Agadir, the increase is approximately 3.7 %, 6.8 %, and 12.4 % for these same coverage percentages.

In terms of PV output, logically, higher coverage percentages result in greater production. The performance is similar in both locations, but the OPV1 modules achieve higher production due to a better performance ratio. Specifically, OPV1 produces approximately 16 % more compared to OPV2. Production is also influenced by the position of the modules on the greenhouse roof, with higher output observed when the OPV modules are placed on flatter facets. For the same coverage percentage, the production from OPV modules positioned at a 10° inclination is 7 % higher than those at 30°, and 17 % higher than those at 45°. For instance, when applying a coverage of 66 % to the greenhouse, the electricity production for the configuration 2OPV10_30 is 4.54 % higher than that for 2OPV10_45, and 8.49 % higher than for 2OPV30_45. Fig. 12 illustrates the overall energy demand (determined by subtracting

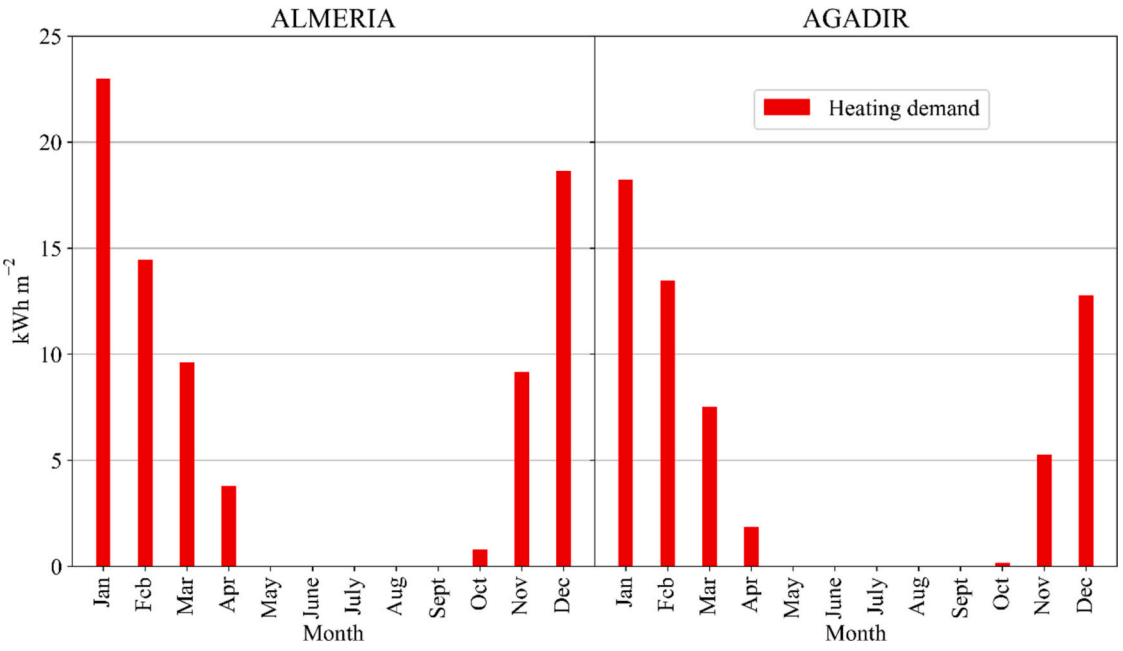

Fig. 11. Monthly heating demand of the reference greenhouse (Almeria and Agadir).

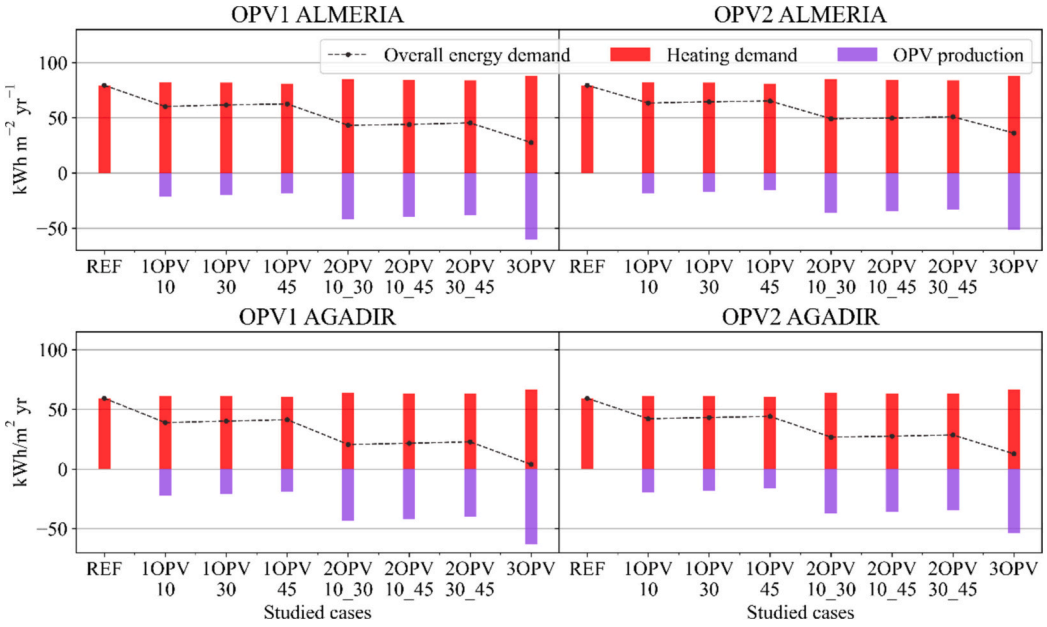

Fig. 12. Annual heating demand (Almeria; Agadir), considering different configurations.

the annual energy produced by the OPV cells (if installed) to the annual heating demand). Even with a heating system that has a coefficient of performance (COP), which is the ratio of heat delivered out of the energy consumed, of 1. OPV1 can cover up to 36 %, 67 %, and 94 % of the thermal demand with the coverage percentages of 33 %, 66 %, and 100 % in Agadir, and 26 %, 49 %, and 70 % in Almeria, respectively. With OPV2, due to reduced electricity production, the thermal demand covered by electricity production amounts to 31 %, 58 %, and 80 % in Agadir, and 22 %, 42 %, and 58 % in Almeria.

5.2. Light level and distribution

The hourly results of illumination at crop level obtained from Radiance-Daysim have been seasonally analysed through boxplots (see Fig. 13). This approach enabled a visual depiction of the distribution of DLI values within the control zone of the greenhouse. This approach enabled us to observe both the mean value and the variance in light levels across the study area.

Results indicate that an increase the coverage percentage by the OPVs leads to a decrease in the mean DLI. It has been observed that OPV2 allows a higher flow of photons to reach the plant canopy compared to OPV1, contrary to what is observed in the production of electrical energy. This fact is due to the higher transmittance of OPV's, and the higher the amount of photons passing through the cell the lower the electricity produced. Additionally, considering the regional climatology, Agadir experiences a greater photon flux during the winter and autumn than Almeria, while the reverse is true for the spring and summer periods.

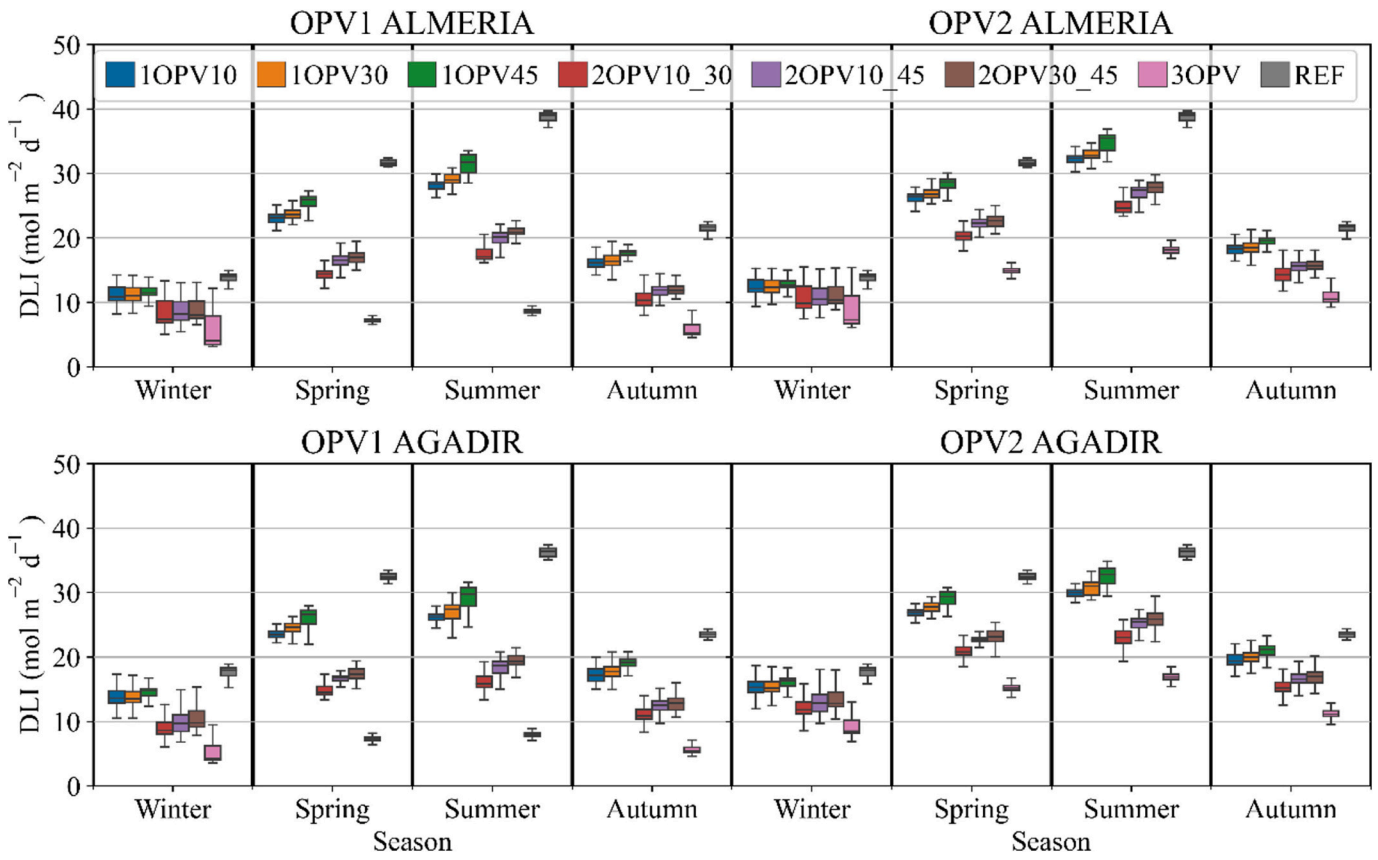

Fig. 13. Average seasonal DLI at the plant-canopy level (Almeria; Agadir), considering different configurations.

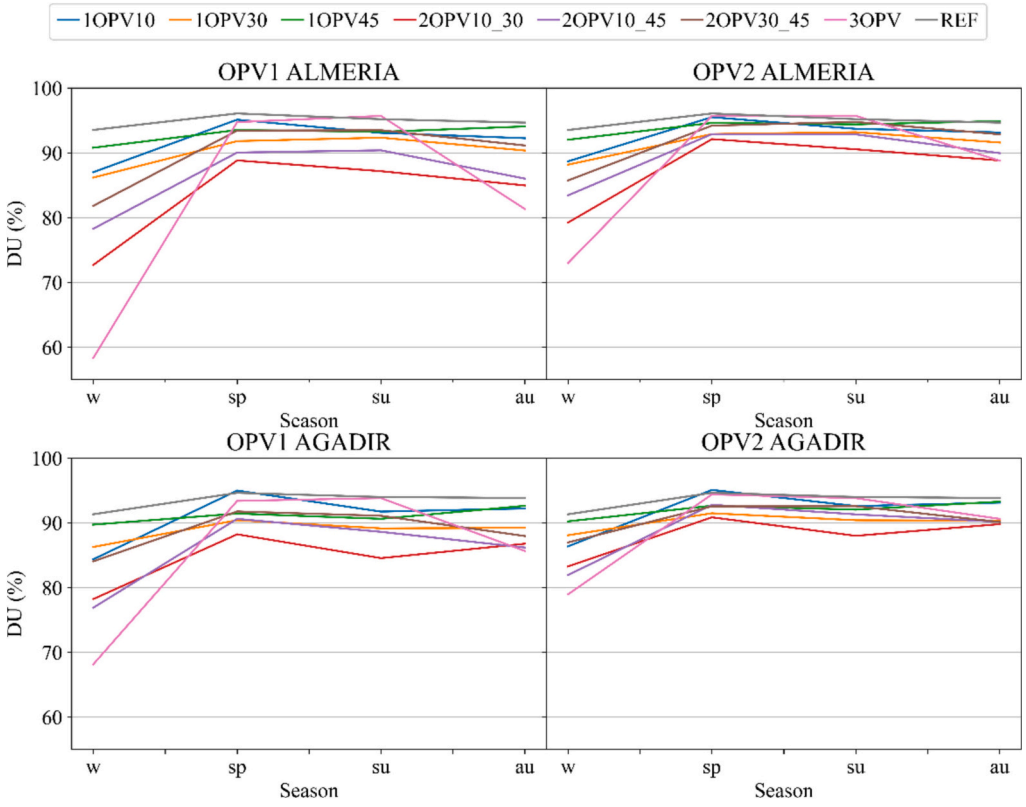

Fig. 14. Uniformity of the radiation inside the zone control of the greenhouse evaluated through the Distribution Uniformity (DU) (by season; w = winter, sp. = spring, su = summer, au = autumn).

Going into further detail, observations in both locations demonstrate that the optimal coverage percentage can vary. This variation depends on the season and the type of OPV. During winter periods, when the coverage percentage by OPVs exceeds 33 %, the DLI experiences a significant decrease, falling below the recommended ranges for seedling growth, which are 13–16 mol m^{-2} d^{-1} [99]. In autumn, spring and summer this significant decrease in DLI occurs with 100 % coverage by OPV1. For the other cases, the DLI reaches higher values. When analysing the DLI in comparison to the reference case (ETFE), a coverage percentage of 33 % results in a light reduction in the range of 15 % to 25 % for OPV1 and 7 % to 17 % for OPV2. With a coverage percentage of 66 %, the reduction in light falls within the range of 40 % to 54 % for OPV1 and 23 % to 36 % for OPV2. When the coverage percentage reaches 100 % with OPVs, the reduction ranges from 58 % to 77 % for OPV1 and 36 % to 53 % for OPV2 (See more in Supplementary Table 1). It's worth noting that the highest reduction is consistently achieved in all cases when the modules are positioned with a flatter orientation.

Regarding lighting uniformity, it is observed that during the winter months, all configurations show a larger difference between the minimum and maximum DLI values, which can be attributed to the border effects of the greenhouse. The light uniformity of the different configurations has been confirmed through the distribution of the lighting uniformity (DU), as shown in Fig. 14. The influence of OPV coverage on light uniformity shows significant seasonal variation. Configurations with 33 % and 66 % OPV coverage demonstrate reduced homogeneity, while full roof coverage with OPV modules generally improves light distribution, except in winter when the lower sun angle reduces light penetration through the south vertical walls (see supplementary Fig. 1). Notably, DU decreases during the summer months as the steeper solar angle increases the contrast between light and shaded areas within the greenhouse. This contrast is less pronounced with 100 % OPV coverage, whereas configurations with lower shading exhibit greater variability in light distribution.

5.3. Crop yield

The simulated plant weight depicted in Fig. 15 has been calculated for a large crop cycle spanning 262 days (from the 1st of January to the 19th of September). Based on the analysis of light availability, the introduction of the OPVs as a greenhouse cover reduces the DLI, thereby affecting the overall crop weight. When using OPV1 technology, this reduction in crop weight is more pronounced, aligning with the previously indicated reduction in photon flux transmitted to the crop. Similar trends have been observed in both Almeria and Agadir. With a coverage percentage of 33 % using OPV1, the reduction in crop weight is approximately 7 %, while with OPV2, it decreases to 5 %. At a coverage percentage of 66 %, the reduction in crop weight reaches approximately 19 % for OPV1 and around 12 % for OPV2. Finally, when OPVs cover the entire greenhouse (100 % coverage), the reductions are more pronounced, with a decrease of 41 % for OPV1 and 23 % for OPV2.

6. Conclusions

The present study evaluates the integration of two semitransparent OPV modules in a multi-tunnel greenhouse located in two typical regions known for greenhouse-based agriculture: Almeria and Agadir. Thermal dynamics, electricity generation, lighting conditions, and tomato crop behaviour have been modelled for various greenhouse configurations. In terms of energy performance, the findings show that incorporating OPVs, especially with higher coverage percentages on the greenhouse roof, results in increased heating demand due to reduced solar energy entry. However, this is offset by a rise in electricity. However, this effect is counteracted by an increased electricity production. Solar fractions of about 25 %, 50 %, and 75 % in Almeria, and 30 %, 65 %, and 90 % in Agadir have been obtained for OPVs coverage percentage of 33 %, 66 %, and 100 %, respectively, considering a heating system with a COP of 1.

The greenhouse lighting performance has been analysed by evaluating the mean seasonal DLI. Results indicate that DLI values decrease below the minimum required levels when increasing the coverage percentage with OPV modules. The ideal coverage percentage varies by season and depends on the type of OPV module used. For instance, during winter, DLI is significantly reduced when the coverage percentage exceeds 33 % for both types of modules. Conversely, in spring and summer, these modules maintain good levels of illumination, whereas in autumn, the lower transmittance of OPV1 modules results in poorer illumination. It is also important to highlight the significance of considering uniformity indices in the evaluation of lighting performance. The results show some differences depending on the configuration, the period of the year, and the study area considered.

The results show a direct correlation between crop weight and lighting levels in the PAR region. Therefore, a reduction in crop yield has

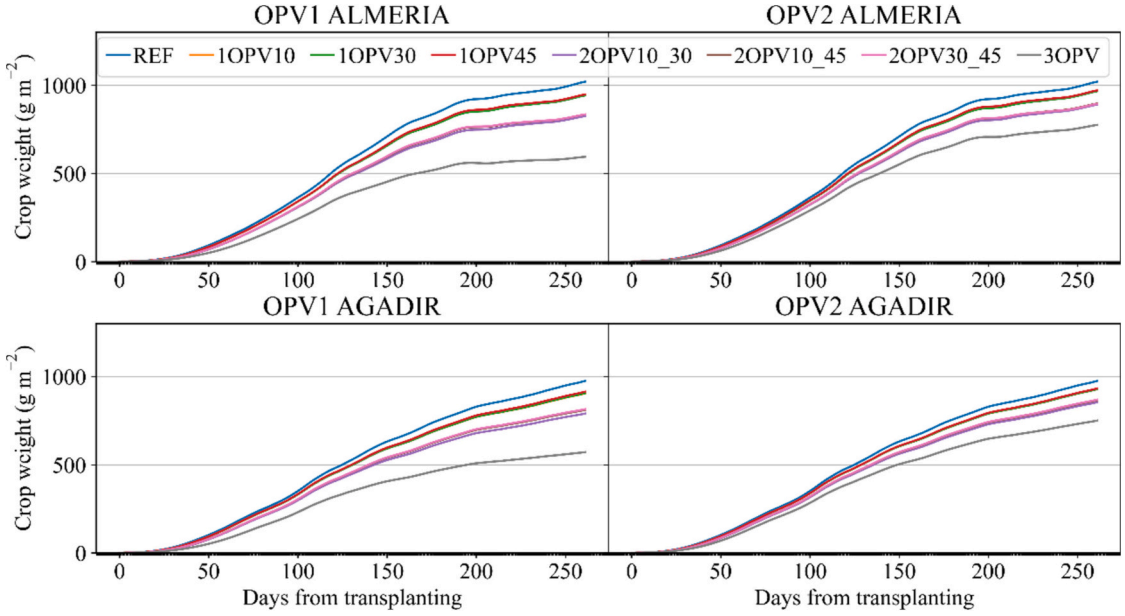

Fig. 15. Simulated tomato crop weight vs. days after transplanting (Almeria; Agadir), considering different configurations.

been observed when integrating OPVs. This reduction is more pronounced with OPV1 technology compared to OPV2 since AVT values are 17.8 % and 21.8 %, respectively. For instance, with a coverage percentage of 33 %, using OPV1 modules, crop weight was reduced by 7 %, whereas OPV2 led to a slightly lesser 5 % reduction. Increasing the coverage percentage to 66 % caused a more significant decline, approximately 19 % for OPV1 and 12 % for OPV2. The most substantial impact has been noted when the greenhouse was fully covered (100 % coverage percentage) with OPV modules, leading to reduction values in crop weight of 41 % (OPV1) and 23 % (OPV2).

In conclusion, integrating semitransparent OPVs into greenhouse structures has implications for heating demand, electricity production, light levels, and crop yield. The selection of OPV technology, the coverage percentage, and the positioning of modules are key to balancing energy production with optimal crop growth in these systems. The opposite tendency between energy performance and crop production scenarios presents a significant challenge in determining the optimal solution. In response to this, a strategy that slightly favours food production is adopted to minimise the impact on crop growth. From this perspective, in both locations the coverage percentage of 33 % by two technologies presents a reasonable compromise, minimising the reduction in crop yield while still contributing to the greenhouse needs. Also is remarkable that the technology OPV2 with the coverage percentage of 66 % could offer a suitable solution maintaining the reduction in crop yield below the 12 %.

However, based on these results, we are not in a position to definitively determine the optimal solution. This decision requires take into account the agriculturist's perspective and the specific characteristics of each farm to assess whether the reduction in crop yield is adequately compensated by energy savings and other factors.

This study provides a comprehensive methodology for analysing greenhouses equipped with semitransparent OPVs, contributing to the need for more uniform and standardised approaches in the field of agrivoltaics. This methodology highlights the importance of consistent modelling tools, boundary conditions, and clearly defined metrics. By offering these insights, the work supports the ongoing development of standardised practices, which are essential for enabling more accurate comparisons and promoting advancements across different agrivoltaic systems and studies.

We are currently conducting experimental studies to validate and refine our model further. Although this work lacks direct experimental validation, we have ensured a relative measure of reliability by consistently comparing our results with a reference case. These upcoming experimental studies and the application of the present methodology to several locations with diverse weather conditions, will serve to strengthen and improve the accuracy and applicability of our conclusions. In addition, future research on cost scenarios for greenhouse-integrated organic PVs will provide a more complete assessment of its long-term viability and economic impact.

CRediT authorship contribution statement

A. Moreno: Writing – original draft, Visualization, Validation, Software, Methodology, Investigation, Conceptualization. **D. Chemisana:** Writing – review & editing, Validation, Supervision, Project administration, Methodology, Investigation, Funding acquisition, Conceptualization. **E.F. Fernández:** Writing – review & editing, Supervision, Project administration, Methodology, Funding acquisition, Conceptualization.

Declaration of competing interest

The authors declare that they have no known competing financial interests or personal relationships that could have appeared to influence the work reported in this paper.

Acknowledgements

The authors would like to thank the **Spanish MCIN/AEI/10.13039/501100011033** for the funding (grant reference: PID2019-111536RB-I00; TED2021-132843B-I00; PLEC2022-009435). Alex Moreno Bellostes is a Serra Húnter Fellow. D. Chemisana thanks Institució Catalana de Recerca i Estudis Avançats (ICREA) for the ICREA Acadèmia award. Furthermore, this research was supported by the *Generalitat de Catalunya* (2021 SGR 01618).

Appendix A. Supplementary data

Supplementary data to this article can be found online at https://doi.org/10.1016/j.apenergy.2025.125285.

Data availability

Data will be made available on request.

References

[1] Nonhebel S. Renewable energy and food supply: will there be enough land? Renew Sustain Energy Rev 2005;9:191–201.
[2] Le Mouël C, Forslund A. How can we feed the world in 2050? A review of the responses from global scenario studies. Eur Rev Agric Econ 2017;44:541–91.
[3] Bremmer J, Riemens M, Reinders M. The future of crop protection in Europe. 2021. ISBN 9789284676842.
[4] Rockström J, Steffen W, Noone K, Persson Å, Chapin FS, Lambin EF, et al. A safe operation space for humanity. Nature 2009;461:472–5.
[5] Rockström J, Gupta J, Qin D, Lade SJ, Abrams JF, Andersen LS, et al. Safe and just earth system boundaries. Nature 2023;619:102–11.
[6] Campbell BM, Beare DJ, Bennett EM, Hall-Spencer JM, Ingram JSI, Jaramillo F, et al. Agriculture production as a major driver of the earth system exceeding planetary boundaries. Ecol Soc 2017;22.
[7] Dupraz C, Marrou H, Talbot G, Dufour L, Nogier A, Ferard Y. Combining solar photovoltaic panels and food crops for optimising land use: towards new agrivoltaic schemes. Renew Energy 2011;36:2725–32.
[8] Goetzberger A, Zastrow A. On the coexistence of solar-energy conversion and plant cultivation. Int J Sol Energy 1982;1:55–69.
[9] Barron-Gafford GA, Pavao-Zuckerman MA, Minor RL, Sutter LF, Barnett-Moreno I, Blackett DT, et al. Agrivoltaics provide mutual benefits across the food–energy–water nexus in drylands. Nat Sustain 2019;2:848–55.
[10] Chalgynbayeva A, Gabnai Z, Lengyel P, Pestisha A, Bai A. Worldwide research trends in Agrivoltaic systems—a bibliometric review. Energies 2023;16:1–25.
[11] Sekiyama T, Nagashima A. Solar sharing for both food and clean energy production: performance of agrivoltaic systems for corn, a typical shade-intolerant crop. Environ - MDPI 2019:6.
[12] Willockx B, Uytterhaegen B, Ronsijn B, Herteleer B, Cappelle J. A standardized classification and performance indicators of Agrivoltaic systems. Eu Pvsec 2020; 2020:1–4.
[13] Macknick J, Hartmann H, Barron-gafford G, Beatty B, Burton R, Choi CS, et al. The 5 Cs of Agrivoltaic success factors in the United States. Lessons From the InSPIRE Research Study 2022:80.
[14] Carrausse R, Arnauld de Sartre X. Does agrivoltaism reconcile energy and agriculture? Lessons from a French case study. Energy Sustain Soc 2023;13:1–14.
[15] Von Elsner B, Briassoulis D, Waaijenberg D, Mistriotis A, Von Zabeltitz C, Gratraud J, et al. Review of structural and functional characteristics of greenhouses in European Union countries, part II: typical designs. J. Agric. Eng. Res. 2000;75: 111–26.
[16] Pastuszak J, Węgierek P. Photovoltaic cell generations and current research directions for their development. Materials (Basel) 2022:15.
[17] Moretti S, Marucci A. A photovoltaic greenhouse with variable shading for the optimization of agricultural and energy production. Energies 2019:12.
[18] Marucci A, Zambon I, Colantoni A, Monarca D. A combination of agricultural and energy purposes: evaluation of a prototype of photovoltaic greenhouse tunnel. Renew Sustain Energy Rev 2018;82:1178–86.
[19] Cossu M, Yano A, Murgia L, Ledda L, Deligios PA, Sirigu A, et al. Effects of the photovoltaic roofs on the greenhouse microclimate. Acta Hortic 2017;1170:461–8.
[20] Cossu M, Murgia L, Ledda L, Deligios PA, Sirigu A, Chessa F, et al. Solar radiation distribution inside a greenhouse with south-oriented photovoltaic roofs and effects on crop productivity. Appl Energy 2014;133:89–100.
[21] Kadowaki M, Yano A, Ishizu F, Tanaka T, Noda S. Effects of greenhouse photovoltaic array shading on welsh onion growth. Biosyst. Eng. 2012;111:290–7.
[22] Yano A, Furue A, Kadowaki M, Tanaka T, Hiraki E, Miyamoto M, et al. Electrical energy generated by photovoltaic modules mounted inside the roof of a north-south oriented greenhouse. Biosyst. Eng. 2009;103:228–38.
[23] Guadalupe L, Carreño-ortega A, Fatnassi H, Poncet C. The effect of different levels of shading in a photovoltaic greenhouse with a north–south orientation. 2020.

[24] Thompson EP, Bombelli EL, Shubham S, Watson H, Everard A, D'Ardes V, et al. Tinted semi-transparent solar panels allow concurrent production of crops and electricity on the same cropland. Adv Energy Mater 2020;10:1–9.
[25] Glass SAS. Analysis of the viability of a photovoltaic greenhouse with. 2021.
[26] Lu SM, Amaducci S, Gorjian S, Haworth M, Ha C, Ma T, et al. Review Wavelength-selective solar photovoltaic systems to enhance spectral sharing of sunlight in agrivoltaics 2024:2483–522.
[27] Vu H, Tien TQ, Park J, Cho M, Vu NH, Shin S. Waveguide concentrator photovoltaic with spectral splitting for dual land use. Energies 2022:15.
[28] Sonneveld PJ, Swinkels GLAM, Campen J, van Tuijl BAJ, Janssen HJJ, Bot GPA. Performance results of a solar greenhouse combining electrical and thermal energy production. Biosyst. Eng. 2010;106:48–57.
[29] Bicer Y, Sajid MU, Al-Breiki M. Optimal spectra management for self-power producing greenhouses for hot arid climates. Renew Sustain Energy Rev 2022;159:112194.
[30] Loik ME, Carter SA, Alers G, Wade CE, Shugar D, Corrado C, et al. Wavelength-selective solar photovoltaic systems: powering greenhouses for plant growth at the food-energy-water Nexus. Earth's Futur 2017;5:1044–53.
[31] Hayali A, Reeves RJ, Alkaisi MM. Wavelength selective solar cells using triple cation perovskite. Nanomaterials 2022:12.
[32] Liu Y, Keil J, Ferry VE, Kortshagen UR. Energy and thermal performance analysis of quantum dot luminescent solar concentrators in greenhouses. Adv Sustain Syst 2023;2300107:1–11.
[33] Lu L, Ya'acob ME, Anuar MS, Chen G, Othman MH, Noor Iskandar A, et al. Thermal analysis of a portable DSSC mini greenhouse for botanical drugs cultivation. Energy Rep 2020;6:238–53.
[34] Roslan N, Ya'acob ME, Radzi MAM, Hashimoto Y, Jamaludin D, Chen G. Dye sensitized solar cell (DSSC) greenhouse shading: new insights for solar radiation manipulation. Renew Sustain Energy Rev 2018;92:171–86.
[35] Fu J, Fong PWK, Liu H, Huang CS, Lu X, Lu S, et al. 19.31% binary organic solar cell and low non-radiative recombination enabled by non-monotonic intermediate state transition. Nat Commun 2023:14.
[36] Li Y, Guo X, Peng Z, Qu B, Yan H, Ade H, et al. Color-neutral, semitransparent organic photovoltaics for power window applications. Proc Natl Acad Sci U S A 2020;117:21147–54.
[37] Zhao Y, Zhu Y, Cheng H-W, Zheng R, Meng D, Yang Y. A review on semitransparent solar cells for agricultural application. Mater Today Energy 2021;22:100852.
[38] Meitzner R, Schubert US, Hoppe H. Agrivoltaics—the perfect fit for the future of organic photovoltaics. Adv. Energy Mater. 2021:11.
[39] Wang D, Liu H, Li Y, Zhou G, Zhan L, Zhu H, et al. High-performance and eco-friendly semitransparent organic solar cells for greenhouse applications. Joule 2021;5:945–57.
[40] dos Reis Benatto GA, Corazza M, Roth B, Schütte F, Rengenstein M, Gevorgyan SA, et al. Inside or outside? Linking outdoor and indoor lifetime tests of ITO-free organic photovoltaic devices for greenhouse applications. Energ Technol 2017;5:338–44.
[41] Zisis C, Pechlivani EM, Tsimikli S, Mekeridis E, Laskarakis A, Logothetidis S. Organic photovoltaics on greenhouse rooftops: effects on plant growth. Mater Today Proc 2020;21:65–72.
[42] Friman-Peretz M, Ozer S, Geoola F, Magadley E, Yehia I, Levi A, et al. Microclimate and crop performance in a tunnel greenhouse shaded by organic photovoltaic modules – comparison with conventional shaded and unshaded tunnels. Biosyst. Eng. 2020;197:12–31.
[43] Ravishankar E, Charles M, Xiong Y, Henry R, Swift J, Rech J, et al. Balancing crop production and energy harvesting in organic solar-powered greenhouses. Cell Reports Phys Sci 2021;2:100381.
[44] Waller R, Kacira M, Magadley E, Teitel M, Yehia I. Semi-transparent organic photovoltaics applied as greenhouse shade for spring and summer tomato production in arid climate. Agronomy 2021;11:1–20.
[45] Magadley E, Kabha R, Dakka M, Teitel M, Friman-Peretz M, Kacira M, et al. Organic photovoltaic modules integrated inside and outside a polytunnel roof. Renew Energy 2022;182:163–71.
[46] Ukwu UN, Agbo JU, Muller O, Schrey S, Nedbal L, Niu Y, et al. Effect of organic photovoltaic and red-foil transmittance on yield, growth and photosynthesis of two spinach genotypes under field and greenhouse conditions. Photosynth Res 2023;157:103–18.
[47] Charles M, Edwards B, Ravishankar E, Calero J, Henry R, Rech J, et al. Emergent molecular traits of lettuce and tomato grown under wavelength-selective solar cells. Front Plant Sci 2023;14:1–16.
[48] Okada K, Yehia I, Teitel M, Kacira M. Crop production and energy generation in a greenhouse integrated with semi-transparent organic photovoltaic film. Acta Hortic. 2018;1227:231–9.
[49] Mukrimaa SS, Nurdyansyah, Fahyuni EF, Yulia Citra A, Schulz ND, Taniredja T, et al. No 主観的健康感を中心とした在宅高齢者における 健康関連指標に関する共分散構造分析Title. J Penelit Pendidik Guru Sekol Dasar 2016;6:128.
[50] Ravishankar E, Booth RE, Saravitz C, Sederoff H, Ade HW, O'Connor BT. Achieving net zero energy greenhouses by integrating semitransparent organic solar cells. Joule 2020;4:490–506.
[51] Waller R, Kacira M, Magadley E, Teitel M, Yehia I. Evaluating the performance of flexible, semi-transparent large-area organic photovoltaic arrays deployed on a greenhouse. AgriEngineering 2022;4:969–92.
[52] Safat Dipta S, Schoenlaub J, Habibur Rahaman M, Uddin A. Estimating the potential for semitransparent organic solar cells in agrophotovoltaic greenhouses. Appl Energy 2022;328:120208.
[53] Ravishankar E, Booth RE, Hollingsworth JA, Ade H, Sederoff H, DeCarolis JF, et al. Organic solar powered greenhouse performance optimization and global economic opportunity. Energ Environ Sci 2022;15:1659–71.
[54] Goudriaan J. H.H.L. Modelling Potential Crop Growth Processes2; 1994 [ISBN 9780792332206.].
[55] Moreno A, Chemisana D, Lamnatou C, Maestro S. Energy and photosynthetic performance investigation of a semitransparent photovoltaic rooftop greenhouse for building integration. Renew Energy 2023;118976.
[56] Vanhaelewyn L, Van Der Straeten D, De Coninck B, Vandenbussche F. Ultraviolet radiation from a plant perspective: the plant-microorganism context. Front Plant Sci 2020;11:1–18.
[57] Mormile P, Rippa M, Graziani G, Ritieni A. Use of greenhouse-covering films with tailored UV-B transmission dose for growing 'medicines' through plants: rocket salad case. J Sci Food Agric 2019;99:6931–6.
[58] Abdel-Ghany AM, Al-Helal IM, Alzahrani SM, Alsadon AA, Ali IM, Elleithy RM. Covering materials incorporating radiation-preventing techniques to meet greenhouse cooling challenges in arid regions: a review. Sci World J 2012;2012.
[59] Liu J, van Iersel MW. Photosynthetic physiology of blue, green, and red light: light intensity effects and underlying mechanisms. Front Plant Sci 2021:12.
[60] McCree KJ. The action spectrum, absorptance and quantum yield of photosynthesis in crop plants. Agric Meteorol 1971;9:191–216.
[61] Stefani L, Zanon M, Modesti M, Ugel E, Vox G, Schettini E. Reduction of the environmental impact of plastic films for greenhouse covering by using fluoropolymeric materials. Acta Hortic. 2008;801 PART 1:131–7.
[62] ASCA® | Organic solar film (OPV) - Transparent and flexible Available online, https://en.asca.com (accessed on Sep 23, 2023).
[63] Hengevoss D, Baumgartner C, Nisato G, Hugi C. Life Cycle Assessment and eco-efficiency of prospective, flexible, tandem organic photovoltaic module. Sol. Energy 2016;137:317–27.
[64] Emmott CJM, Röhr JA, Campoy-Quiles M, Kirchartz T, Urbina A, Ekins-Daukes NJ, et al. Organic photovoltaic greenhouses: a unique application for semi-transparent PV? Energ Environ Sci 2015;8:1317–28.
[65] Inada K. Action spectra for photosynthesis in higher plants. Plant Cell Physiol 1976;17:355–65.
[66] Stallknecht EJ, Herrera CK, Yang C, King I, Sharkey TD, Lunt RR, et al. Designing plant – transparent agrivoltaics. Sci Rep 2023:1–14.
[67] Bugbee B. Toward an optimal spectral quality for plant growth and development : the importance of radiation capture. 2016. p. 1–12.
[68] Katz EA, Faiman D, Tuladhar S. Temperature dependence for the photovoltaic device parameters of polymer- fullerene solar cells under operating conditions temperature dependence for the photovoltaic device parameters of polymer-fullerene solar cells under operating conditions. 2001.
[69] Bardizza G, Salis E, Toledo C, Dunlop ED. Power performance and thermal operation of organic photovoltaic modules in real operating conditions. 2020. p. 593–600.
[70] Moreno A, Riverola A, Chemisana D, Vaillon R, Solans A. Design and characterization of an OPV-ETFE multi-layer semi-transparent glazing. Energy Rep 2022;8:8312–20.
[71] Klein S, Beckman W. TRNSYS 18: A transient system simulation program: Mathematical reference. 2017.
[72] Berkeley L. WINDOW 7 user manual. 2019.
[73] Ward G. F.R. A new technique for computer simulation of illuminated spaces. 1988.
[74] Holmgren FW, Hansen WC, Mikofski AM. Pvlib Python: a Python package for modeling solar energy systems. J Open Source Softw 2018;3:884.
[75] Jones JW, Dayan E, Allen LH, Van Keulen H, Challa H. Dynamic tomato growth and yield model (TOMGRO). Trans Am Soc Agric Eng 1991;34:663–72.
[76] Remund J, Kunz S. *Meteonorm : global meteorological database for solar energy and applied climatology*; Ed. '97, version 3.0.; Meteotest: Bern, Switzerland SE - 1 computer optical disc ; 4 3/4 in. 1997.
[77] Cañadas JJM, Fernández ÁBL, Juan JJPP, Hernández JCL. Invernaderos con cubierta de plástico y cristal en el sureste español 2008:1–54.
[78] Torrellas M, Torrellas M, Antón A, López JC, Baeza EJ, Parra JP, et al. LCA of a tomato crop in a multi-tunnel greenhouse in Almeria. 2012.
[79] Mendoza-Fernández AJ, Peña-Fernández A, Molina L, Aguilera PA. The role of technology in greenhouse agriculture: towards a sustainable intensification in campo de dalías (Almería, Spain). Agronomy 2021;11:1–14.
[80] S, J.A. Heliyon. Carbon capture from biomass flue gases for CO 2 enrichment in greenhouses10; 2024.
[81] Kottek M, Grieser J, Beck C, Rudolf B, Rubel F. World map of the Köppen-Geiger climate classification updated. eschweizerbartxxx Meteorol Zeitschrift 2006;15:259–63.
[82] Ahemd HA, Al-faraj AA, Abdel-ghany AM. Scientia Horticulturae Shading greenhouses to improve the microclimate, energy and water saving in hot regions : A review201; 2016. p. 36–45.
[83] Gueymard C. SMARTS2, A simple model of the atmospheric radiative transfer of sunshine: algorithms and performance assessment. Fsec-Pf-270-95 1995:78.
[84] Fernández EF, Villar-Fernández A, Montes-Romero J, Ruiz-Torres L, Rodrigo PM, Manzaneda AJ, et al. Global energy assessment of the potential of photovoltaics for greenhouse farming. Appl Energy 2022;309.
[85] Van Beveren PJM, Bontsema J, Van Straten G, Van Henten EJ. Minimal heating and cooling in a modern rose greenhouse. Appl Energy 2015;137:97–109.
[86] Monteith J. Evaporation and environment. Symposia of the Society for Experimental Biology. Symp Soc Exp Biol 1965:205–34.
[87] Kittas C, Boulard T, Mermier M, Papadakis G. Wind induced air exchange rates in a greenhouse tunnel with continuous side openings. J Agric Eng Res 1996;65:37–49.

[88] Molina-Aiz FD, Valera DL, Peña AA, Gil JA, López A. A study of natural ventilation in an Almería-type greenhouse with insect screens by means of tri-sonic anemometry. Biosyst Eng 2009;104:224–42.
[89] Pérez D, Soler M, Delgado M, Reigada A. Science of the Total environment energy use and carbon footprint of the tomato production in heated multi-tunnel greenhouses in Almeria within an exporting Agri-food system context. Sci Total Environ 2018;628–629:1627–36.
[90] FAO, F. And A.O. Of the U. Land & Water Available online, https://www.fao.org/land-water/databases-and-software/crop-information/tomato/en/#c236455 (accessed on Sep 2, 2024).
[91] Perez R, Ineichen P, Seals R, Michalsky J, Stewart R. Modeling daylight availability and irradiance components from direct and global irradiance. Sol Energy 1990;44:271–89.
[92] Perez R, Seals R, Michalsky J. All-weather model for sky luminance distribution-preliminary configuration and validation. Sol. Energy 1993;50:235–45.
[93] Ashdown I. Photometry and photosynthesis : from photometry to PPFD (revised). Photometry and Photosynthesis. 2015 (accessed on 13 September 2024). Available online: https://www.researchgate.net/publication/284157299_Photometry_and_Photosynthesis_From_Photometry_to_PPFD_Revised.
[94] Torrente J, Reca J, Rafael L. Simulation model to analyze the spatial distribution of solar radiation in agrivoltaic Mediterranean greenhouses and its effect on crop water needs353; 2024.
[95] Jones JW, Kenig A, Vallejos CE. Reduced state-variable tomato growth model. Trans Am Soc Agric Eng 1999;42:255–65.
[96] Prieto J, Ajnannadhif RM, Fernández-del Olmo P, Coronas A. Integration of a heating and cooling system driven by solar thermal energy and biomass for a greenhouse in Mediterranean climates. Appl Therm Eng 2023;221.
[97] López JC, Pérez-Parra J, Baille A, Bonachela S. Effects of heating strategies on earliness and yield of snap beans (Phaseolus vulgaris L.) grown under "Parral" plastic greenhouses. Acta Hortic. 2003;614:439–44.
[98] Choab N, Allouhi A, El Maakoul A, Kousksou T, Saadeddine S, Jamil A. Effect of greenhouse design parameters on the heating and cooling requirement of greenhouses in Moroccan climatic conditions. IEEE Access 2021;9:2986–3003.
[99] Gómez C, Mitchell CA. Growth responses of tomato seedlings to different spectra of supplemental lighting. HortScience 2015;50:112–8.